Title

An evaluation of the variable-resolution CESM for modeling California's climate

Journal

Journal of Advances in Modeling Earth Systems, 8(1)

ISSN

1942-2466

Authors

Huang, Xingying
Rhoades, Alan M
Ullrich, Paul A
et al.

Publication Date

2016-03-01

DOI

10.1002/2015ms000559

Peer reviewed

AGU PUBLICATIONS

Journal of Advances in Modeling Earth Systems

RESEARCH ARTICLE

10.1002/2015MS000559

An evaluation of the variable-resolution CESM for modeling California's climate

Xingying Huang[1], Alan M. Rhoades[1], Paul A. Ullrich[1], and Colin M. Zarzycki[2]

[1]Department of Land, Air and Water Resources, University of California, Davis, California, USA, [2]National Center for Atmospheric Research, Boulder, CO

Key Points:
- Variable-resolution GCMs provide a means to access regional scales in a global modeling system
- VR-CESM, a variable-resolution GCM, is able to accurately model regional climate over California
- For temperature and precipitation, VR-CESM demonstrates competitive solution quality to a RCM (WRF)

Supporting Information:
- Figure S1
- Figure S2
- Figure S3
- Figure S4
- Figure S5
- Figure S6
- Figure S7
- Figure S8
- Figure S9
- Figure S10
- Figure S11
- Figure S12
- Figure S13
- Figure S14
- Figure S15
- Figure S16
- Figure S17
- Figure S18
- Figure S19
- Figure S20
- Figure S21
- Figure S22
- Figure S23
- Figure S24
- Figure S25
- Figure S26
- Figure S27

Correspondence to:
X. Huang,
xyhuang@ucdavis.edu

Citation:
Huang, X., A. M. Rhoades, P. A. Ullrich, and C. M. Zarzycki (2016), An evaluation of the variable-resolution-CESM for modeling California's climate, *J. Adv. Model. Earth Syst.*, *8*, 345–369, doi:10.1002/2015MS000559.

Received 8 OCT 2015
Accepted 8 FEB 2016
Accepted article online 10 FEB 2016
Published online 18 MAR 2016

Abstract In this paper, the recently developed variable-resolution option within the Community Earth System Model (VR-CESM) is assessed for long-term regional climate modeling of California at 0.25° (∼28 km) and 0.125° (∼14 km) horizontal resolutions. The mean climatology of near-surface temperature and precipitation is analyzed and contrasted with reanalysis, gridded observational data sets, and a traditional regional climate model (RCM)—the Weather Research and Forecasting (WRF) model. Statistical metrics for model evaluation and tests for differential significance have been extensively applied. With only prescribed sea surface temperatures, VR-CESM tended to produce a warmer summer (by about 1–3°C) and overestimated overall winter precipitation (about 25%–35%) compared to reference data sets. Increasing resolution from 0.25° to 0.125° did not produce a statistically significant improvement in the model results. By comparison, the analogous WRF climatology (constrained laterally and at the sea surface by ERA-Interim reanalysis) was ∼1–3°C colder than the reference data sets, underestimated precipitation by ∼20%–30% at 27 km resolution, and overestimated precipitation by ∼65–85% at 9 km. Overall, VR-CESM produced comparable statistical biases to WRF in key climatological quantities. This assessment highlights the value of variable-resolution global climate models (VRGCMs) in capturing fine-scale atmospheric processes, projecting future regional climate, and addressing the computational expense of uniform-resolution global climate models.

1. Introduction

Global climate models (GCMs) have been widely used to simulate both past and future climate. Although these models have demonstrable success in representing large-scale features of the climate system, they are usually employed at relatively coarse resolutions (∼1°), largely as a result of the substantial computational cost required at higher resolutions. Global climate reanalysis data sets, which assimilate climate observations using a global model, represent a best estimate of historical weather patterns. However, reanalysis data sets still cannot fulfill the needs of policymakers, stakeholders, and researchers that require high-resolution regional climate data (http://reanalyses.org/atmosphere/overview-current-reanalyses). Regional features such as microclimates, land cover, and topography are not well captured by either GCMs or reanalysis data sets [*Leung et al*., 2003a]. However, dynamical processes at unrepresented scales are significant drivers for local climate variability, especially over complex terrain [*Soares et al*., 2012]. In order to capture fine-scale dynamical features, high horizontal resolution is needed for a more accurate representation of small-scale processes and interactions [*Rauscher et al*., 2010]. With these enhancements, regional climate data are expected to be more useful for formulating climate adaptation and mitigation strategies locally.

In order to model regional climate at high spatial resolutions over a limited area, downscaling techniques have been developed, such as statistical and dynamical downscaling. Dynamical downscaling typically uses nested limited-area models (LAMs) or, more recently, variable-resolution enabled GCMs (VRGCMs) [*Laprise*, 2008]. In this context, LAMs are typically referred to as regional climate models (RCMs) when used for climate study. Forced by the output from GCMs or reanalysis data sets, RCMs have been widely used to capture physically consistent regional and local circulations at the needed spatial and temporal scales [*Christensen et al*., 2007; *Bukovsky and Karoly*, 2009; *Mearns et al*., 2012]. Recently, there has been a growing interest in the use of VRGCMs for modeling regional climate. Unlike RCMs, VRGCMs use a relatively coarse global model with enhanced resolution over a specific region [*Staniforth and Mitchell*, 1978; *Fox-Rabinovitz*

et al., 1997]. Strategies that have been employed for transitioning between coarse and fine-resolution regions within a VRGCM include grid stretching [*Fox-Rabinovitz et al*., 1997; *McGregor and Dix*, 2008] and grid refinement [*Ringler et al*., 2008; *Skamarock et al*., 2012; *Zarzycki et al*., 2014a]. VRGCMs have demonstrated utility for regional climate studies and applications at a reduced computational cost compared to uniform-resolution GCMs [*Fox-Rabinovitz et al*., 2006; *Rauscher et al*., 2013; *Zarzycki et al*., 2015].

Compared with RCMs, a key advantage of VRGCMs is that they use a single, unified modeling framework, rather than two separate models (GCM and RCM) with potentially disparate dynamics and physics parameterizations. RCMs may suffer from potential inconsistencies between the global and regional scales and lack two-way interactions at the nest boundary [*Warner et al*., 1997; *McDonald*, 2003; *Laprise et al*., 2008; *Mesinger and Veljovic*, 2013], which can be mitigated with the use of VRGCMs. VRGCMs also provide a cost-effective method of reaching high resolutions over a region of interest—the limited-area simulations in this study at 0.25° and 0.125° resolution represent a reduction in required computation of approximately 10 and 25 times, respectively, compared to analogous globally uniform high-resolution simulations. For the purposes of this paper, we focus on the recently developed Community Earth System Model with variable-resolution option (VR-CESM) as our VRGCM of interest. This configuration is driven by the Community Atmosphere Model's (CAM's) Spectral Element (SE) dynamical core, which possesses attractive conservation and parallel scaling properties [*Dennis et al*., 2012; *Taylor*, 2011], as well as recently developed variable-resolution capabilities [*Zarzycki et al*., 2014a; *Zarzycki and Jablonowski*, 2015]. This model has been employed by *Zarzycki et al*. [2014b] to show that a high-resolution refinement patch in the Atlantic basin for simulating tropical cyclones represented significant improvements over the unrefined simulation. *Zarzycki et al*. [2015] also compared the large-scale climatology of VR-CESM 0.25° and uniform CESM at 1° and found that adding a refined region over the globe did not noticeably affect the global circulation. *Rhoades et al*. [2015] have also assessed the use of VR-CESM for modeling Sierra Nevada mountain snowpack in the western United States.

However, for the purposes of long-term regional climate modeling, particularly in regions where high-resolution is anticipated to be most beneficial, VR-CESM has yet to be rigorously evaluated. This paper aims to fill that gap by analyzing the performance of VR-CESM against gridded observational data, reanalysis product and in comparison to a traditional RCM forced by reanalysis data. Our variable-resolution simulations are implemented with horizontal resolutions of 0.25° and 0.125°, respectively, which are much more typical for dynamically downscaled studies. This paper focuses on California in the western United States as the study area. The complex topography and coastlines of California strongly modulate large-scale weather patterns, creating local climatic features such as coastal fog, sea breeze, mountain-induced precipitation, and snowpack. An understanding of local climate variability in California is incredibly important for policymakers and stakeholders due to its vast agricultural industry, mixed demographics, and vulnerability to anthropogenically induced climate change [*Hayhoe et al*., 2004; *Cayan et al*., 2008]. Consequently, we expect that California is an excellent test bed for regional climate modeling.

In this study, the Weather Research and Forecasting (WRF) [*Skamarock et al*., [2005] model has been used for simulating California's climatology at 27 and 9 km grid spacing. RCM simulations over California have also been conducted in previous studies and demonstrated the need for high spatial and temporal resolution to better address regional climate and extreme events, especially in the vicinity of complex topography where large climatological gradients are present [*Leung et al*., 2004; *Kanamitsu and Kanamaru*, 2007; *Caldwell et al*., 2009; *Pan et al*., 2011; *Pierce et al*., 2013]. In particular, *Caldwell et al*. [2009] presented results from WRF at 12 km spatial resolution and showed that, although the RCM was effective at simulating the mean climate when compared with observations, some clear biases persisted (particularly an overestimation of precipitation).

This study focuses on the models' ability to represent current climate statistics, particularly those relevant to heat and precipitation extremes. We anticipate that this work will validate VR-CESM for modeling the mean regional climatology of California and will further motivate the adoption of variable-resolution modeling to study other local climatic processes. Our eventual goal is to utilize these models for assessing historical and future regional climate extremes.

This paper is organized as follows: section 2 describes the model setup, data sets, and methodology for evaluation and intercomparison. In section 3, simulation results are provided and discussed, with focuses on near-surface (2 m) temperature and precipitation. Key results are summarized along with further discussion in section 4.

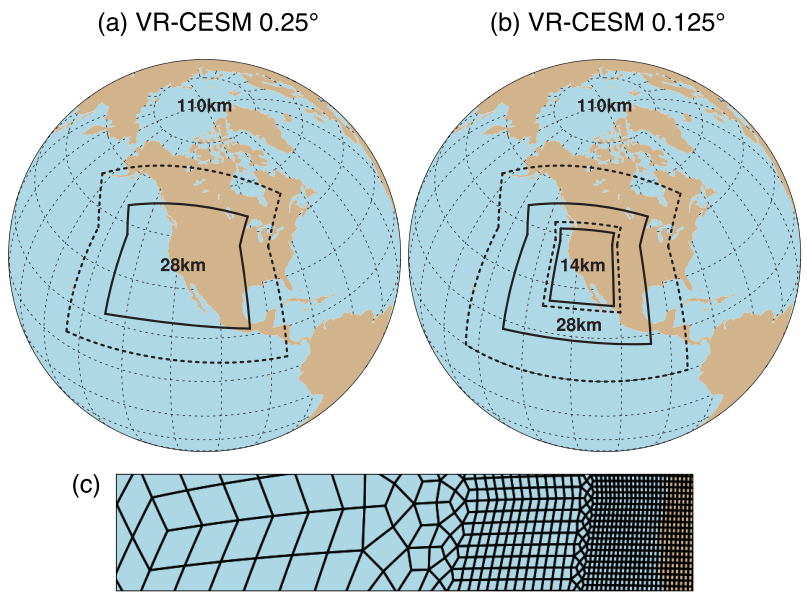

Figure 1. The approximate grid spacing in the (a) VR-CESM 0.25° and (b) VR-CESM 0.125° meshes used in this study. (c) A depiction of the transition from the global 1° resolution mesh through two layers of refinement to 0.25° and again to 0.125°.

2. Models and Methodology

2.1. Simulation Design

In this study, all global simulations use the Atmospheric Model Intercomparison Project (AMIP) experimental protocols [*Gates*, 1992]. These protocols are widely used and support climate model diagnosis, validation, and intercomparison. AMIP experiments are constrained by realistic sea surface temperatures (SSTs) and sea ice from 1979 to near present without the added complexity of ocean-atmosphere feedbacks in the climate system. In particular, observed SSTs and sea ice at 1° horizontal resolution are provided and updated following the procedure described by *Hurrell et al*. [2008].

2.1.1. VR-CESM

CESM is a state-of-the-art Earth modeling framework managed by the National Center for Atmospheric Research (NCAR), consisting of coupled atmospheric, oceanic, land, and sea ice models. For decades CESM (and its predecessor, the Community Climate System Model) has been used for modeling present and future global climate [*Neale et al*., 2010a; *Hurrell et al*., 2013]. The coupling infrastructure in CESM communicates the interfacial states and fluxes between each component model to ensure conservation. Since we follow AMIP protocols, only the atmosphere and land model are integrated dynamically. Here CAM version 5 (CAM5) [*Neale et al*., 2010b] and the Community Land Model (CLM) version 4.0 [*Oleson et al*., 2010] are used. As mentioned earlier, the SE dynamical core is employed along with variable-resolution grid support. The FAMIPC5 (F _ AMIP _ CAM5) component set, which mainly supports atmospheric, oceanic, land, and sea ice models, is chosen for these simulations. In CAM5, cloud microphysics is parameterized using the two-moment scheme with ice supersaturation [*Morrison and Gettelman*, 2008; *Gettelman et al*., 2008], and the deep convection process is treated by Zhang and McFarlane (ZM) cumulus scheme [*Zhang and McFarlane*, 1995]. A more detailed discussion of the CAM5 configuration can be found in *Neale et al*. [2010a].

For our study, the variable-resolution cubed-sphere grids are generated for use in CAM and CLM with the open-source software package SQuadGen [*Ullrich*, 2014; *Guba et al*., 2014]. The grids used in this study are depicted in Figure 1. The maximum horizontal resolution on these grids is 0.25° (∼28 km) and 0.125° (∼14 km), respectively, with a quasi-uniform 1° mesh over the remainder of the globe. Grids are constructed using a paving technique with a 2:1 spatial resolution ratio, so two transition layers are required from 1° to 0.25°, and one additional transition from 0.25° to 0.125°. In our study, and previous studies [e.g., *Zarzycki et al*., 2015], general circulation patterns (e.g., wind, pressure, and precipitation) do not exhibit apparent artifacts in the variable-resolution transition region, and the design of the SE dynamical core ensures that dry air and tracer mass are conserved globally [*Taylor and Fournier*, 2010]. Simulations are performed over the

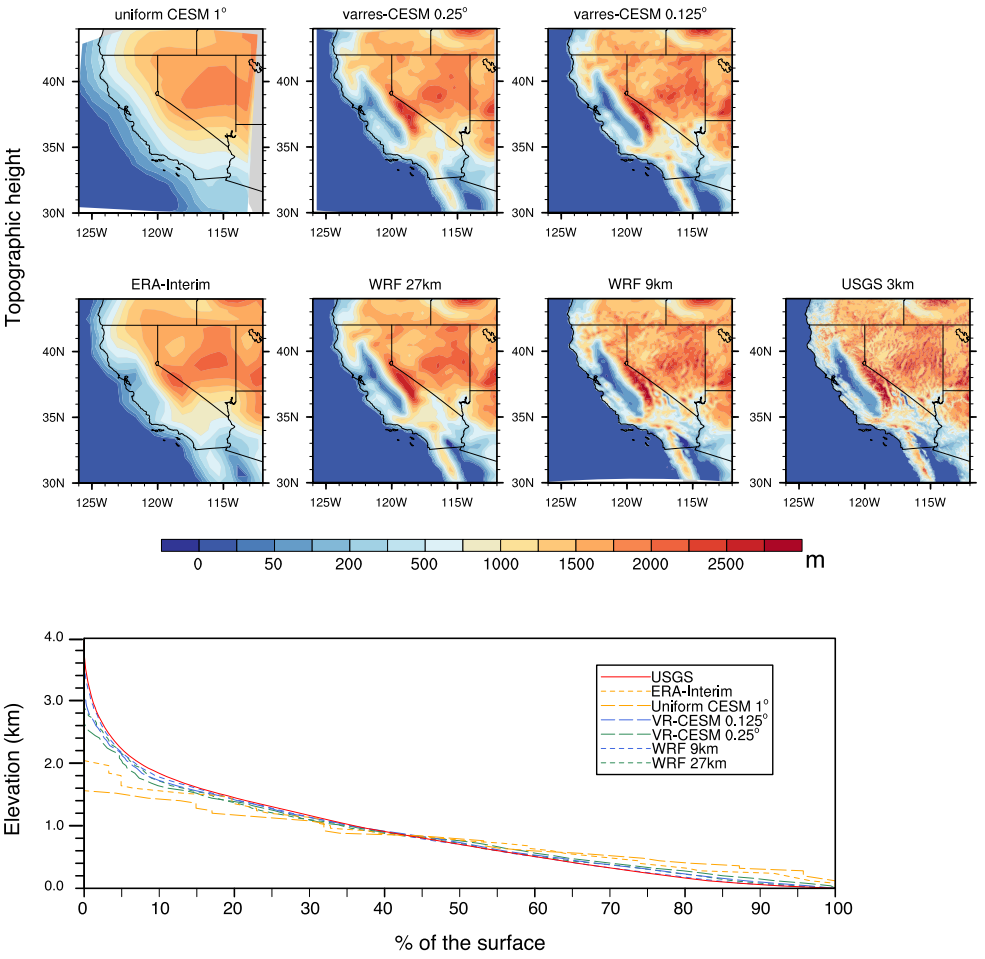

Figure 2. (top) Topographic heights (from top left to bottom right) for VR-CESM 0.25°, VR-CESM 0.125°, uniform CESM 1°, WRF 27 km, WRF 9 km, ERA-Interim ($\Delta x \sim 80$ km), and USGS (~3 km). (bottom) Hypsometric curves for the above data sets over California.

time period from 1 January 1979 to 31 December 2005 (UTC) and year 1979 is discarded as a spin-up period. This 26 year time period is chosen to provide an adequate sampling of interannual variability, to limit computational cost, and to coincide with the satellite era where adequate high-quality gridded and reanalysis data sets are available.

Variable-resolution topography files were produced by sampling the National Geophysical Data Center (NGDC) 2 min (~4 km) Gridded Global Relief Data set (ETOPO2v2), followed by the application of a differential smoothing technique as described in *Zarzycki et al.* [2015]. Using this technique, the *c* parameter from their equation (1) was adjusted to reduce noise in the vertical pressure velocity field. The grid-scale topography is depicted in Figure 2, including the topography of uniform CESM at 1° and observed topography from USGS 2 min (3 km) data set. Hypsometric curves, depicting the percentage of the California region above a given elevation, are plotted in Figure 2 for models and observations. It is apparent that higher resolution provides clear improvement in the representation of regional topography, which is necessary for the correct treatment of fine-scale dynamic processes strongly influenced by complex terrain. Topography at very coarse resolution (~1°) is too smooth to represent local details like the shape of valleys or mountain peaks, resulting in the loss of regional climate patterns.

Land surface data sets, including plant functional types, at 0.5° were adopted. Greenhouse gas (GHG) concentrations and aerosol forcings are prescribed based on historical observations. CAM and CLM tuning parameters are not modified from their default configurations.

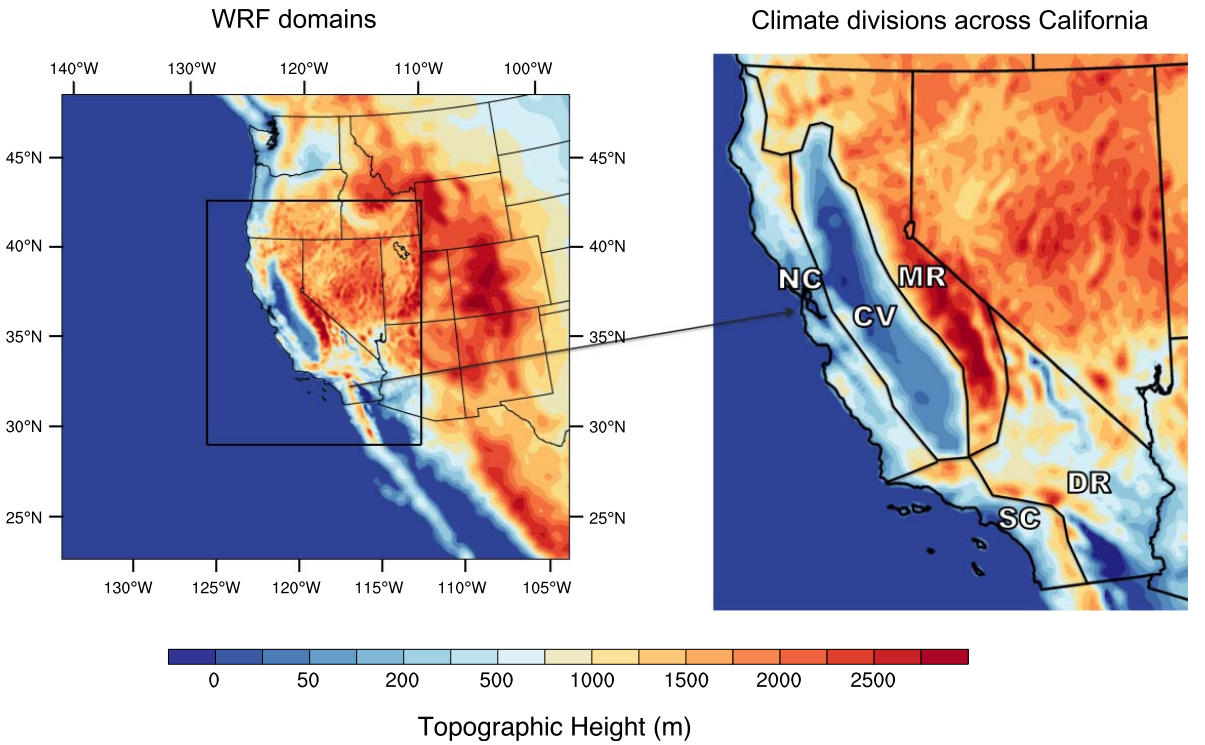

Figure 3. (left) WRF 27 km (entire plot region) and WRF 9 km (solid black box) simulation domains. (right) Five climate divisions for California. Both plots are overlaid with WRF model topography.

2.1.2. WRF

WRF has been widely used over the past decade for modeling regional climate [*Lo et al*., 2008; *Leung and Qian*, 2009; *Soares et al*., 2012; *Sun et al*., 2015]. In our study, the fully compressible nonhydrostatic WRF model (version 3.5.1) with the Advanced Research WRF (ARW) dynamical core is used. WRF is a limited-area model that supports nested domains with a typical refinement ratio of 3:1. The simulation domains of WRF are depicted in Figure 3. Two WRF simulations, representing finest grid resolutions of 27 and 9 km, are conducted. For the WRF 27 km simulation, one domain is used. For the WRF 9 km simulation, two domains are used, with the outer domain at 27 km (same as the WRF 27 km) and an inner nested domain at 9 km horizontal grid resolution. For both simulations, grids are centered on California and have 120 × 110 and 151 × 172 grid points, respectively. At all lateral boundaries, 10 grid points are used for relaxation to the coarse solution. In order to reduce the drift between forcing data and modeling output, grid nudging [*Stauffer and Seaman*, 1990] is applied to the outer domain every 6 h at all levels except approximate planetary boundary layers (PBL), as suggested by *Lo et al*. [2008]. The nudging is applied to the wind, temperature, and water vapor mixing ratio with default nudging coefficients. Grid nudging is commonly used and maturely supported in WRF. Although there is evidence spectral nudging may improve the quality of the simulations, an investigation of these differences is out of scope for this paper [*Liu et al*., 2012]. This setup uses 41 vertical levels with model top pressure at 50 hPa.

Additionally, the following physics parameterizations are employed: WSM (WRF Single-Moment) six-class graupel microphysics scheme [*Hong and Lim*, 2006], Kain-Fritsch cumulus scheme [*Kain*, 2004], CAM shortwave and longwave radiation schemes [*Collins et al*., 2004]. These settings are chosen by assessing the results from several common parameterization combinations over a 1 year trial period, which were then compared to gridded observations. For the boundary layer, the Yonsei University scheme (YSU) [*Hong et al*., 2006] is used, and the Noah Land Surface Model [*Chen and Dudhia*, 2001] is applied. Both are chosen as they are common for climate applications that balance long-term reliability and computational cost. Although many other options and parameterization combinations are available for configuring WRF (and others have tackled a complete assessment of these options for particular problems), our choices are made simply to represent a typical WRF configuration. We do note that the Kain-Fritsch convective

Table 1. Reanalysis and Gridded Observational Data Sets Used in This Study

Data Source	Variables Used	Spatial Resolution	Temporal Resolution
NARR	Pr, T_s	32 km	Daily, 3-hourly
NCEP CPC	Pr	~28 km (0.25°)	Daily
UW	Pr, T_{min}, T_{max}	~14 km (0.125°)	Daily
PRISM	Pr, T_{min}, T_{max}, T_{avg}	4 km	Monthly
Daymet	Pr, T_{min}, T_{max}	1 km	Daily

parameterization remains active even within the 9 km inner mesh—although this is considered to be in the "gray zone," it had no appreciable impact on simulation results since almost all precipitation emerged from (large-scale) condensation, as discussed in section 4.

ECMWF Reanalysis (ERA-Interim) data at both the surface and multiple pressure levels provides initial and lateral conditions for the domains. The lateral conditions and SSTs are updated every 6 h. ERA-Interim reanalysis (~80 km) has been widely used and validated for its reliability as forcing data [*Dee et al*., 2011]. WRF simulations are conducted over the same time period as VR-CESM (i.e., 1 January 1979 through 31 December 2005 UTC). Again, the year 1979 is used as a spin-up period and is discarded for purposes of analysis. Notably, the ~9 km resolution employed in the innermost domain is finer than most previous studies for long-term climate.

The topography employed for the 27 and 9 km simulations is interpolated from USGS (United States Geological Survey) elevation data with 10 min (~20 km) and 2 min (~4 km) resolution, respectively. The post-processed grid-scale topography is contrasted in Figure 2. Elevation differences between VR-CESM and WRF are irregular and relatively small, except over the Central Valley where VR-CESM has consistently higher values than WRF. This indicates a different methodology for preparation of the topography data set and may also be partly due to the use of the USGS elevation instead of NGDC elevation data sets.

2.2. Gridded and Reanalysis Data Sets

Reanalysis and gridded observational data sets of the highest available quality are employed (see Table 1). Differences between gridded observations can be due to the choice of meteorological stations, interpolation techniques, elevation models, and processing algorithms. Consequently, the use of multiple reference data sets is necessary to understand the underlying uncertainty in the observational data. Detailed descriptions of these data sets are as follows.

NARR. The North American Regional Reanalysis (NARR) is the NCEP (National Centers for Environmental Prediction) high-resolution reanalysis product that provides dynamically downscaled data over North America at ~32 km resolution and 3-hourly intervals from 1979 through present [*Mesinger et al*., 2006]. We note that some inaccuracies have also been identified in NARR, particularly in precipitation fields [*Bukovsky and Karoly*, 2007].

NCEP CPC. This data set provides gauge-based analysis of daily precipitation from the National Oceanic and Atmospheric Administration (NOAA) Climate Prediction Center (CPC). It is a suite of unified precipitation products obtained by combining all information available at CPC via the optimal interpolation objective analysis technique. The gauge analysis covers the Conterminous United States with a fine resolution at 0.25° from 1 January 1948 to 31 December 2006.

PRISM. The Parameter-elevation Regressions on Independent Slopes Model (PRISM) [*Daly et al*., 2008] supports a 4 km gridded data set obtained by taking point measurements and applying a weighted regression scheme that accounts for many factors affecting the local climatology. The data sets include total precipitation and minimum/maximum, (derived) mean temperatures, and dew points. Monthly climatological variables are available for 1895–2014 from the PRISM Climate Group (Oregon State University, http://prism.oregonstate.edu, created 4 February 2004). Notably, PRISM is the United States Department of Agriculture's official climatological data set. PRISM is used as our primary reference data set for model performance evaluation.

UW. The UW daily gridded meteorological data are obtained from the Surface Water Modeling group at the University of Washington [*Maurer et al*., 2002; *Hamlet and Lettenmaier*, 2005]. UW incorporates topographic corrections by forcing the long-term average precipitation to match that of the PRISM data set. The temperature data set is produced in a similar fashion as precipitation, but uses a simple 6.1 K/km lapse rate for topographic effect. The data set is provided at 0.125° horizontal resolution covering the period 1949–2010.

Daymet. Daymet is an extremely high-resolution (1 km) gridded data set with daily outputs of total precipitation, humidity, and minimum/maximum temperature covering 1980–2013 [*Thornton et al*., 1997, 2014]. The data set is produced using an algorithmic technique that ingests point station measurements in conjunction with a truncated Gaussian weighting filter. Some adjustments are made to account for topography. Daymet is available through the Oak Ridge National Laboratory Distributed Active Archive Center (ORNL DAAC).

2.3. Methodology

Near-surface temperature and precipitation have been analyzed over California to assess the performance of VR-CESM in representing the mean climatology. Specifically, our evaluation focuses on daily maximum, minimum, and average near-surface temperatures (T_{max}, T_{min}, and T_{avg}) and daily precipitation (Pr). These variables are key in a baseline climate assessment due to their close relationship with water resources, agriculture, and health. In this context, the biggest impact of weather on California is through heat and precipitation extremes. Since heat extremes dominate during the summer season, we focus on June, July, and August (JJA) for assessment of temperature. On the other hand, since the vast majority of precipitation in California occurs in the winter season, December–January–February (DJF) is emphasized.

In order to adequately account for natural variability of the mean climate, the simulation period must be chosen appropriately [*Solomon*, 2007]. However, the number of simulated years required for adequate climate statistics depends greatly on the regional climate variability and spatial scale. Past studies have used average weather conditions over a 30 year period to ensure sufficient statistics and to avoid imprinting from annual variability [*Dinse*, 2009]. To check that our 26 year simulation period is sufficient, we have examined the interannual variability of mean temperature and precipitation in all simulations and observations over 5, 10, 20, and 25 seasons or years (depicted in the supporting information). We observe that for climatological mean temperature and precipitation, the relevant statistics are effectively converged for a 20 year sample, suggesting that our simulation period is sufficient to adequately capture the interannual variability of these quantities.

The results in section 4 are obtained from simulated and observed data over the period 1980–2005. All data sets have been linearly detrended at each grid point so as to facilitate averaging of all simulation years. It is found that, for annual and JJA near-surface temperature (T_{max}, T_{min}, and T_{avg}), a statistically significant trend is present under the two-tailed *t* statistic with a significance level of 0.05. For T_{min}, the average warming in 26 years is ∼0.6–1 K for observations, ∼0.5 K for VR-CESMs and WRF 27 km, and ∼1.5 K for WRF 9 km. For T_{max}, the average warming is ∼0.3–0.5 K for observations, ∼0.5–0.8 K for VR-CESMs and WRFs. No statistically significant trend has been detected for precipitation.

California consists of a diverse variety of climate regions as a consequence of its rugged topography and large latitudinal extent. The distinct character of these regions is poorly captured in typical coarse global climate simulations [*Abatzoglou et al*., 2009; *Caldwell et al*., 2009]. In order to assess the performance of VR-CESM within each region, the state has been divided into five climate divisions, including the Central Valley (CV), Mountain Region (MR), North Coast (NC), South Coast (SC), and Desert Region (DR). The spatial extent of these divisions is depicted in Figure 3. These five divisions are determined loosely based on the results of *Abatzoglou et al*. [2009] and the climate divisions used by the California Energy Commission. To restrict the analysis in each division, simulations and data sets have been masked to restrict climate variables to each division.

Standard statistical measures have been used to quantify the model performance in comparison with the reference data sets. These include the root-mean-square deviation (RMSD), mean signed difference (MSD), mean relative absolute difference (MRD), and sample standard deviation (*s*). Further, spatial correlation is assessed by computing Pearson product-moment coefficient of linear correlation between climatological means from models and reference data sets. Mathematically, these quantities are written as

$$\mathrm{RMSD}=\sqrt{\frac{1}{N}\sum_{i=1}^{N}(v_i-\hat{v}_i)^2} \qquad \mathrm{MSD}=\frac{1}{N}\sum_{i=1}^{N}(v_i-\hat{v}_i) \tag{1}$$

Table 2. MSD (Left Column Minus Top Row) of JJA Temperature (°C) and DJF Precipitation (mm/d) Between All Reference Data Sets[a]

	PRISM					UW					Daymet				
	MR	CV	DR	SC	NC	MR	CV	DR	SC	NC	MR	CV	DR	SC	NC
JJA T_{min}															
UW	**−2.0**	**−0.5**	−0.3	**−0.4**	**−2.3**										
Daymet	**−1.8**	0.2	−0.2	−0.3	**−4.6**	0.2	**0.8**	0.1	0.1	**−2.3**					
NARR	**2.5**	**2.5**	**3.1**	−0.2	**2.0**	**4.5**	**3.1**	**3.4**	0.2	**4.2**	**4.3**	**2.3**	**3.2**	0.1	**6.5**
JJA T_{max}															
UW	0.3	−0.1	−0.2	**−0.7**	**−2.4**										
Daymet	−0.3	0.4	−0.2	0.2	**−3.7**	−0.6	**0.5**	0.1	**0.9**	**−1.3**					
NARR	**−1.3**	**1.2**	−0.1	**−0.6**	**−3.7**	**−1.7**	**1.2**	0.1	0.1	**−1.3**	**−1.1**	**0.7**	0.1	**−0.7**	0.0
DJF Pr															
UW	−0.2	0.1	0.0	−0.2	−0.2										
Daymet	−0.1	−0.4	−0.0	0.2	0.5	0.1	−0.5	−0.0	0.3	0.8					
NARR	−0.5	−0.4	−0.1	−0.1	**−1.3**	−0.3	−0.5	−0.1	0.1	−1.1	−0.4	−0.0	−0.1	−0.3	**−1.8**
CPC	−0.8	0.0	0.0	−0.1	−1.1	−0.5	−0.1	0.0	0.1	−0.9	−0.6	0.4	0.0	−0.3	**−1.7**

[a]Statistically significant differences are emphasized in bold (95% confidence level).

$$s=\sqrt{\frac{1}{M-1}\sum_{j=1}^{M}(v_j-\bar{v})^2} \qquad \mathrm{MRD}=\left(\sum_{i=1}^{N}|v_i-\hat{v}_i|\right)/\left(\sum_{i=1}^{N}\hat{v}_i\right) \tag{2}$$

where v_i and $\hat{v}_i$ are values from the simulation output and reference data set, respectively; i is the grid point index and N is the total number of grid points over specific regions; j is the simulation year index, M is the total number of simulated years, and $\bar{v}$ is the mean value over all years. Grid point differences are calculated by remapping the reference data sets to the model's output grid using bilinear interpolation. Remapping using patch-based interpolation has also been tested and nearly identical results have been observed. When necessary, the statistical quantities are further averaged over each division.

Throughout the remainder of this paper, Student's t test has been used to test whether two sets of annual, seasonal, or monthly averaged data are the same. F test is applied to test whether the sample variances are equal. These tests are used only when the sample population can be described adequately by a normal distribution, where normality is assessed under the Anderson-Darling test. When the sample populations do not approximately follow a normal distribution, Mann-Whitney-Wilcoxon (MWW) test and Levene's test are employed in lieu of the t test and F test, respectively. All statistical tests are evaluated at the $p = 0.05$ significance level.

Complementary results to this study are provided in the supporting information, including the original grid-refined mesh files, the sensitivity of climatological statistics to choice of time period, the observed time trend, and other seasons not addressed in this paper and corresponding statistics metric tables. Results are also provided with comparison of VR-CESM to the output from a globally uniform CESM run at 0.25° spatial resolution with the finite volume (FV) dynamical core [*Wehner et al*., 2014].

2.4. Uncertainty in Reference Products

To assess uncertainty in the observational and reanalysis products, we have calculated the MSD values among PRISM, UW, and Daymet for seasonally averaged JJA T_{max}, T_{min}, and DJF Pr over the five divisions and tabulated these results in Table 2. Student's t test is employed to determine significances of differences. For T_{max} and T_{min}, gridded observational data sets are different from each other over some divisions. The most pronounced divergences occur in the NC region, with MSD values reaching up to ~4°C, although differences are also apparent for MR T_{min}. Clearly, UW and Daymet have a colder climatology than PRISM. NARR, as a reanalysis data set, is different from the others over most divisions, with overall larger T_{min} and smaller T_{max}. For precipitation, essentially no significant differences are present, especially among PRISM, UW, and Daymet. NARR and CPC (not shown) seem to have slightly lower precipitation values than others.

3. Results

A detailed analysis of temperature and precipitation results from WRF and VR-CESM is provided in this section. A concise summary of key points follows in section 4.

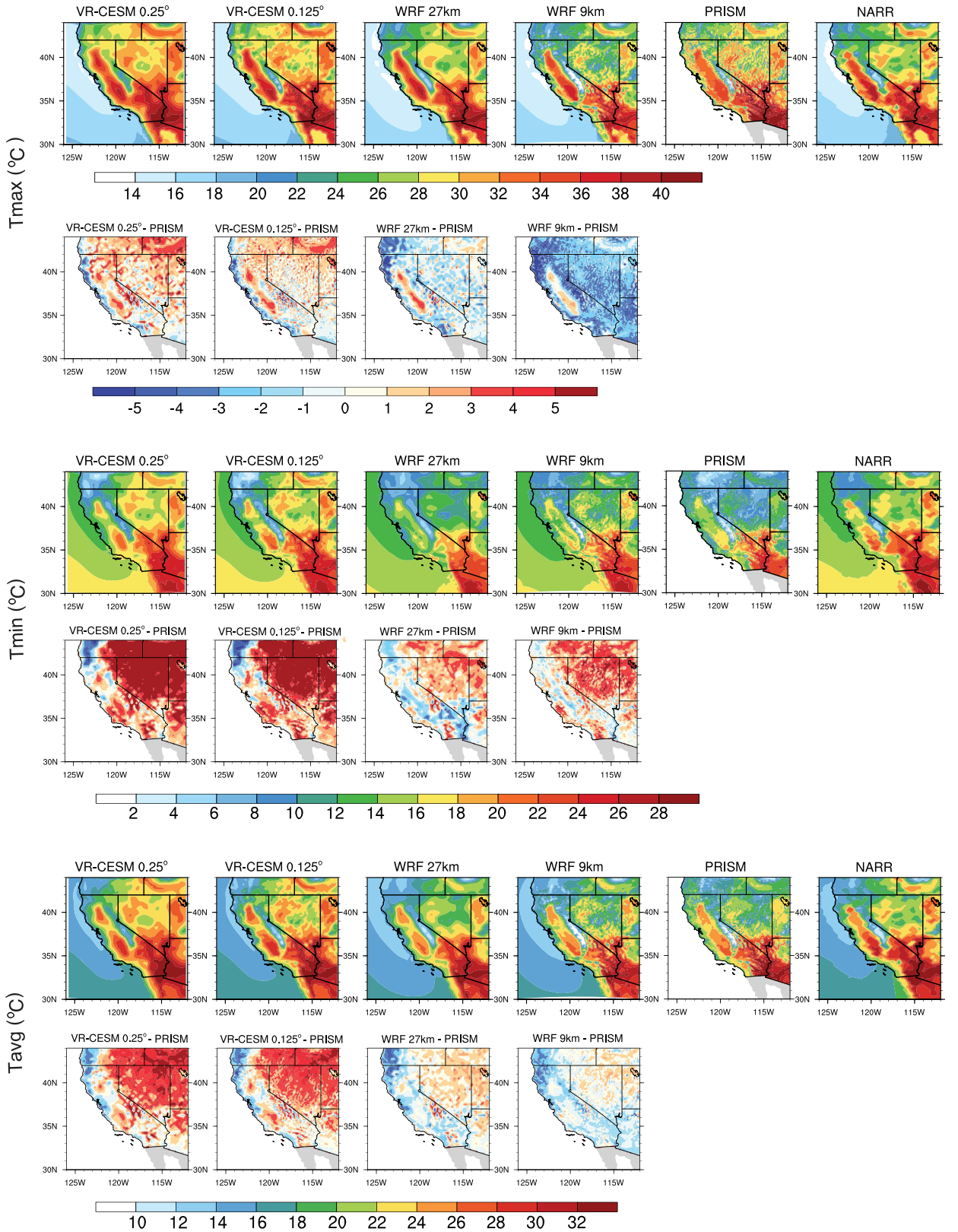

Figure 4. JJA averaged daily T_{max}, T_{min}, and T_{avg} from models and reference data sets, and differences (sharing the same legend) between model results and PRISM.

Table 3. RMSD (°C), MSD (°C), and Spatial Correlation (Corr) for Seasonally Averaged Daily JJA Temperatures Over California

	UW		PRISM			Daymet	
	T_{max}	T_{min}	T_{max}	T_{min}	T_{avg}	T_{max}	T_{min}
RMSD							
VR-CESM 0.25°	2.32	3.75	2.92	3.12	2.60	2.81	3.93
VR-CESM 0.125°	1.90	3.63	2.45	2.94	2.18	2.48	3.70
WRF 27 km	2.31	2.74	2.93	2.25	2.17	2.51	2.99
WRF 9 km	3.32	2.94	3.49	1.84	1.77	3.20	2.94
Uniform CESM 1°	3.06	4.59	3.62	3.43	3.16	3.58	5.07
MSD							
VR-CESM 0.25°	0.98	2.91	0.61	1.73	0.82	1.18	2.88
VR-CESM 0.125°	0.65	2.85	0.20	1.66	0.58	0.82	2.74
WRF 27 km	−0.58	0.82	−0.95	−0.36	−0.77	−0.39	0.79
WRF 9 km	−2.28	1.86	−2.72	0.67	−1.14	−2.10	1.76
Uniform CESM 1°	0.82	3.03	0.60	1.76	1.08	1.24	3.38
Corr							
VR-CESM 0.25°	0.99	0.98	0.99	0.98	0.99	0.99	0.97
VR-CESM 0.125°	0.99	0.98	0.99	0.98	0.99	0.99	0.98
WRF 27 km	0.99	0.98	0.99	0.98	0.99	0.99	0.97
WRF 9 km	0.99	0.98	0.99	0.99	0.99	0.99	0.98
Uniform CESM 1°	0.99	0.96	0.99	0.97	0.99	0.99	0.95

3.1. Temperature

The mean JJA T_{max}, T_{min}, and T_{avg} climatology over the simulation period, together with PRISM and NARR reference data, are plotted in Figure 4. UW and Daymet have not been plotted here since they are visually indistinguishable to PRISM everywhere except for NC, where UW and Daymet exhibit lower temperatures (see Table 2). Statistical measures over California are tabulated in Table 3. In general, all simulations have captured the spatial climate patterns exhibited by PRISM, with high spatial correlations (>0.95), especially for T_{max} and T_{avg}. Nonetheless, several clear biases (relative to PRISM) are present in these simulations, as discussed below.

1. T_{max}: When compared with the reference data sets, VR-CESM showed a warm bias of about 2–3°C in T_{max} over much of the inland domain (CV and MR) and a 2–3°C cool bias along the coast, although the coastal bias is reduced by ∼0.5°C at 0.125° resolution. This is in contrast with WRF, which produced an overall colder climate everywhere except the CV. This bias is especially pronounced for the WRF 9 km simulation, which was approximately 3°C cooler than PRISM. T_{max} within the CV has been overestimated by all the simulations. This likely represents a systematic issue with high-resolution models with respect to California. Possible reasons for this overestimation are discussed at the end of this section.
2. T_{min}: VR-CESM showed a strong warm bias in T_{min} (∼2–4°C), with a particularly large overestimation over Nevada (>5°C). WRF also exhibited a warm bias, but of a much smaller magnitude (∼2–3°C). However, the pattern of T_{min} presented in Figure 4 in both WRF simulations suggests a cooler interior to the CV and warmer perimeter, which is not supported by observations.
3. T_{avg}: The warm bias of T_{min} and T_{max} by VR-CESM resulted in a similar overestimation of T_{avg}. For WRF, underestimation of T_{max} and overestimation of T_{min} led to an overall closer match to T_{avg} over most of the domain but is indicative of a suppressed diurnal cycle.

Compared with the reference data sets over California, VR-CESM 0.125° produced the lowest RMSD values for T_{max}, whereas WRF had smallest RMSD for T_{min}. However, in both cases, the RMSD was around 2°C. Notably, T_{min} from VR-CESM matched much more closely with NARR, although this is likely indicative of a related warm bias in NARR. In fact, closer examination of the differences among VR-CESM, WRF, and NARR marine near-surface temperature patterns indicated that CESM and NARR have T_{min} values that are approximately 2°C larger than WRF. Since coastal near-surface temperature is strongly influenced by ocean SSTs, this difference is likely a key driver of the warm bias in CESM. The Delta breeze effect, which is associated with a sea breeze circulation that brings relatively cool and humid marine air into the interior CV from the San Francisco Bay area, was apparent in all runs. It is especially encouraging that VR-CESM generally performed as well as WRF, in comparison with reference data sets, even though VR-CESM was not constrained or nudged at the lateral boundaries of the high-resolution domain.

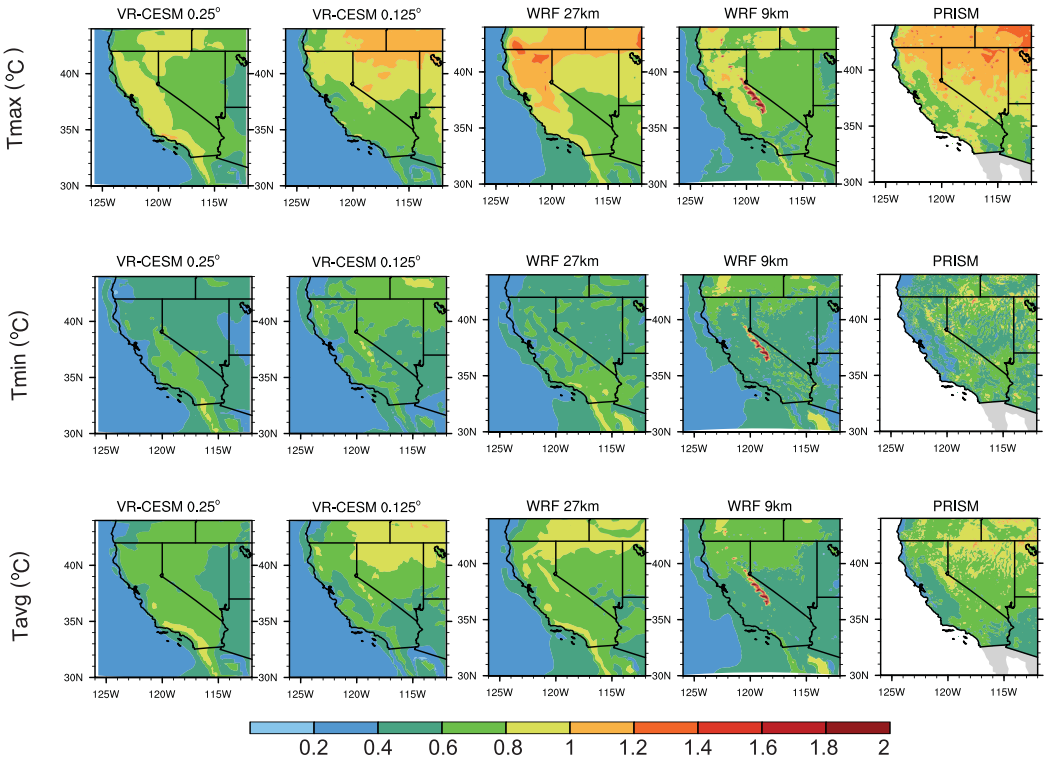

Figure 5. Sample standard deviation of JJA average daily T_{max}, T_{min}, and T_{avg} from model results and PRISM.

The spatial standard deviation of JJA T_{max}, T_{min}, and T_{avg} from models and PRISM is presented in Figure 5. In PRISM, the CV had smaller variability than surrounding regions, although the difference is small (∼0.2°C). Further, areas with rougher topography did exhibit somewhat higher variability than smoother locations. Interestingly, the higher-resolution (0.125°) VR-CESM simulation also matched the spatial pattern and magnitude of standard deviation observed in PRISM, especially for T_{min} and T_{avg}. However, in WRF and VR-CESM 0.25°, the variability is largely consistent across different divisions, and the values are around 0.5–1.5°C for all of the data sets, except for the high Sierras in the WRF 9 km simulation which showed enhanced variability (∼2°C). Compared with reference data sets, the RMSD values of VR-CESM and WRF 27 km are ∼0.1–0.2°C, and ∼0.2–0.3°C for WRF 9 km.

The seasonal cycle of monthly mean T_{avg} in each division is shown in Figure 6 for simulations and for reference data from PRISM and NARR along with the associated 95% confidence interval. PRISM and NARR match closely almost everywhere except in the summer season of NC, SC, and CV, indicative of underlying observational uncertainty. This difference is likely due to the discrepancy in assimilating the coastal cooling effect. In general, model results match closely with reference data with no larger than a 2°C absolute difference, with the largest errors occurring in the summer and winter seasons. Compared with PRISM, VR-CESM overpredicts summer T_{avg} in all divisions except NC and SC and underpredicts winter T_{avg} in all divisions. This corresponds to a larger annual temperature range. WRF has better performance in preserving the monthly cycle when compared with VR-CESM, with about 1°C underestimation over all seasons. There is no clear improvement in the seasonal cycle across resolutions.

Variability in monthly averaged T_{avg} is expressed by the interannual standard deviation of monthly T_{avg} over the 26 year period and is plotted in Figure 7 for the whole California region (results are similar for subregions when renormalized by the mean T_{avg}). The 95% confidence interval obtained from the chi-square test is also depicted for PRISM so as to identify statistically significant differences. RMSD values for monthly standard deviations between models and PRISM are also computed over each climate division (see Table 4). Generally, standard deviation is between 1 and 2°C. Among all models, WRF 27 km is closest to PRISM with RMSD values around 0.1–0.2°C. WRF 9 km is also relatively close to PRISM but exhibits an unusual ∼1°C increase in variability in January and February (statistically significant at the 0.05 level), leading to a

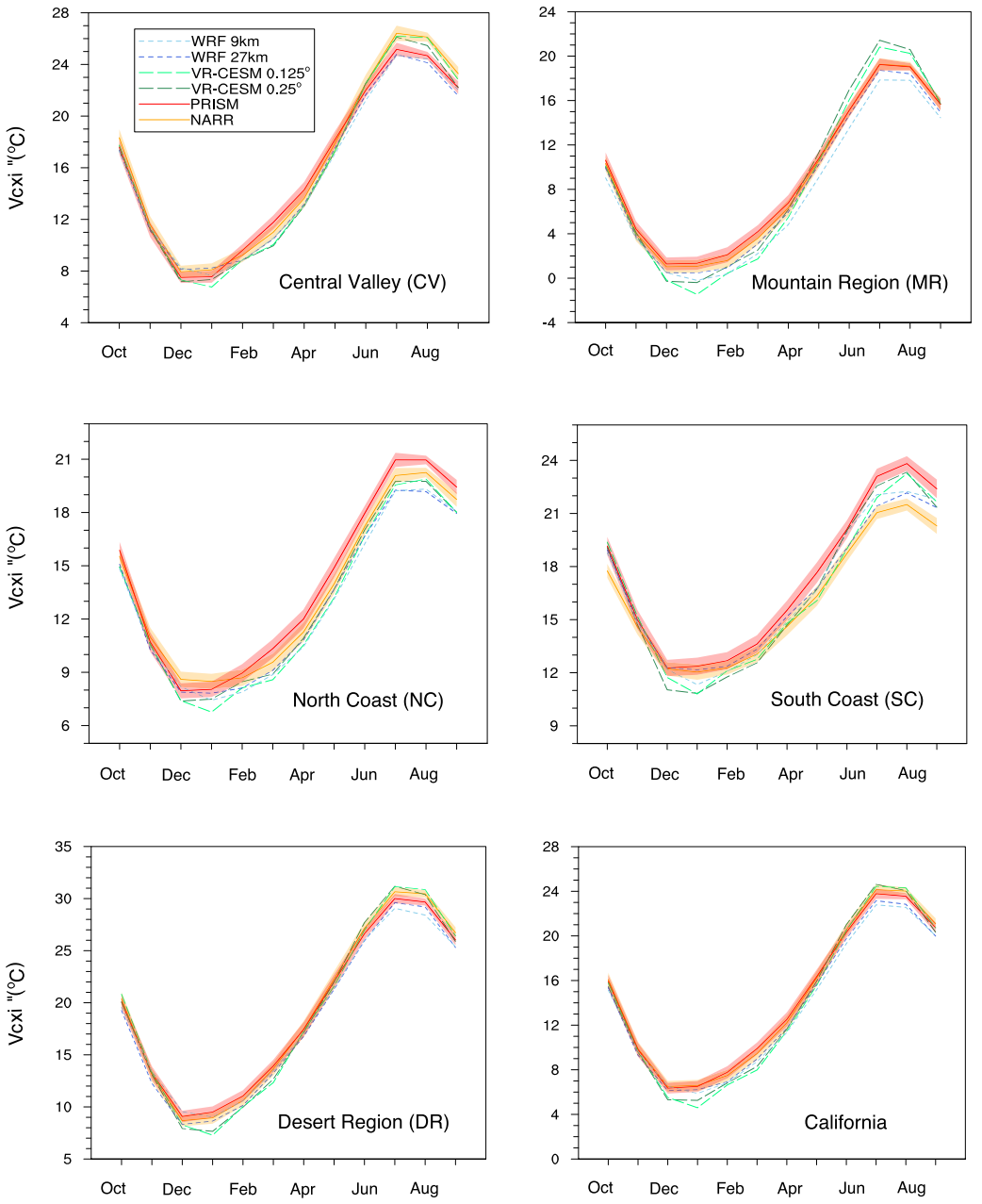

Figure 6. Seasonal cycle of monthly average T_{avg} for each climate division. The shading corresponds to the 95% confidence interval of PRISM and NARR.

relatively high RMSD (~0.5°C). VR-CESM exhibits a weaker correlation with PRISM in all divisions with enhanced variability in DJF and weakened variability in April and May at both resolutions, and in the fall season in the 0.125° simulation, with RMSD around 0.2–0.4°C. This may be indicative of an issue in capturing the seasonality of large-scale Pacific meteorology in CESM and merits further investigation.

Due to the impact of summer heat waves, we now focus on T_{max} over JJA. In Figure 8, the frequency distribution of T_{max} using all JJA daily values at each grid point over 26 years is depicted for models and reference data from UW and Daymet. PRISM is not included since it only deviates from UW and Daymet in the coastal divisions (NC and SC). In these divisions, PRISM is similar in character to UW but shifted several degrees toward warmer temperatures. Properties of the frequency distribution, including average, variability, skewness, and Kurtosis are tabulated in Table 5. As exemplified by the similarity in the moments of the distribution, VR-CESM clearly captures the general distribution of T_{max}. Outside the CV, skewness and

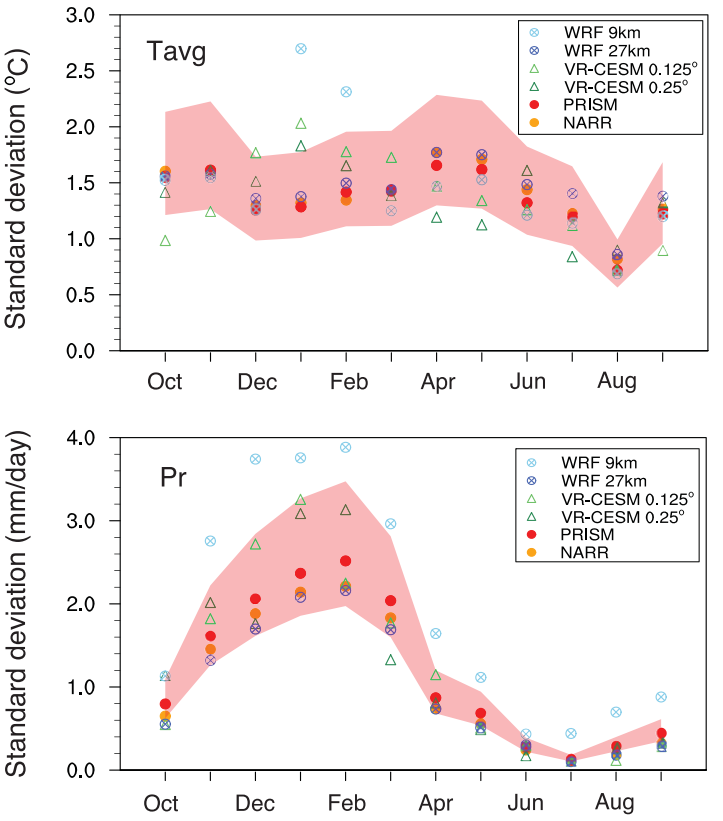

Figure 7. Standard deviation values of monthly average T_{avg} and Pr averaged over California. The shading refers to the 95% confidence interval of PRISM.

kurtosis measures match closely between VR-CESM and the UW data set. In the NC and SC, Daymet overestimates the frequency of very cold days leading to deviation in the moments from UW. Consistent with the observations in Figure 4, outside the CV, WRF tends to be cooler in general and VR-CESM tends to be warmer. In NC and SC, all models more accurately capture the frequency of high T_{max} days than low T_{max} days. Enhanced frequency of cool T_{max} values appears to be the primary driver in overestimation of sample variance in these divisions. For both VR-CESM and WRF, there is no apparent improvement in statistics at higher resolutions.

In the CV, models show a clear warm bias and underestimated skewness, associated with a long forward tail and temperatures approaching near 50°C. As discussed earlier, all models overestimate T_{max} over CV. In order to further assess the accuracy of the gridded observations, we examine the T_{max} data directly from recorded weather station measurements over the CV (obtained from Global Historical Climate Network, provided by the NOAA/NCDC, http://www.ncdc.noaa.gov/). The results validate that T_{max} values above 45°C are rare (although station observations suggest these days may be slightly more frequent than suggested by UW and Daymet). The warm bias associated with the aforementioned extreme hot days in both VR-CESM and WRF is likely correlated with overly dry summertime soil moisture, as discussed in *Caldwell et al.* [2009]. This could be caused by the lack of accurate land surface treatment in climate models—for example, *Bonfils and Lobell* [2007] found that irrigation over CV has decreased summertime maximum temperature by ~2–3 K in heavily irrigated areas compared with nearby nonirrigated areas, based on long-term temperature records. Other studies have also found the cooling effects of irrigation over CV based on model simulations. *Kueppers et al.* [2007], using RegCM3 (the third generation of the Regional Climate Model), found that irrigated areas has been cooled by ~3.7 K in August over the CV.

Table 4. RMSD for the Standard Deviation Values of Monthly Averaged T_{avg}/Pr Between Models and PRISM in Each Climate Division

	MR	CV	DR	SC	NC
T_{avg}					
VR-CESM 0.25°	0.393	0.304	0.231	0.253	0.286
VR-CESM 0.125°	0.468	0.355	0.359	0.275	0.334
WRF 27 km	0.101	0.199	0.129	0.231	0.141
WRF 9 km	0.438	0.561	0.454	0.476	0.536
Pr					
VR-CESM 0.25°	0.449	0.976	0.228	0.517	0.670
VR-CESM 0.125°	0.315	0.848	0.237	0.532	0.499
WRF 27 km	0.193	0.126	0.246	0.494	0.724
WRF 9 km	1.700	1.057	0.425	0.817	0.958

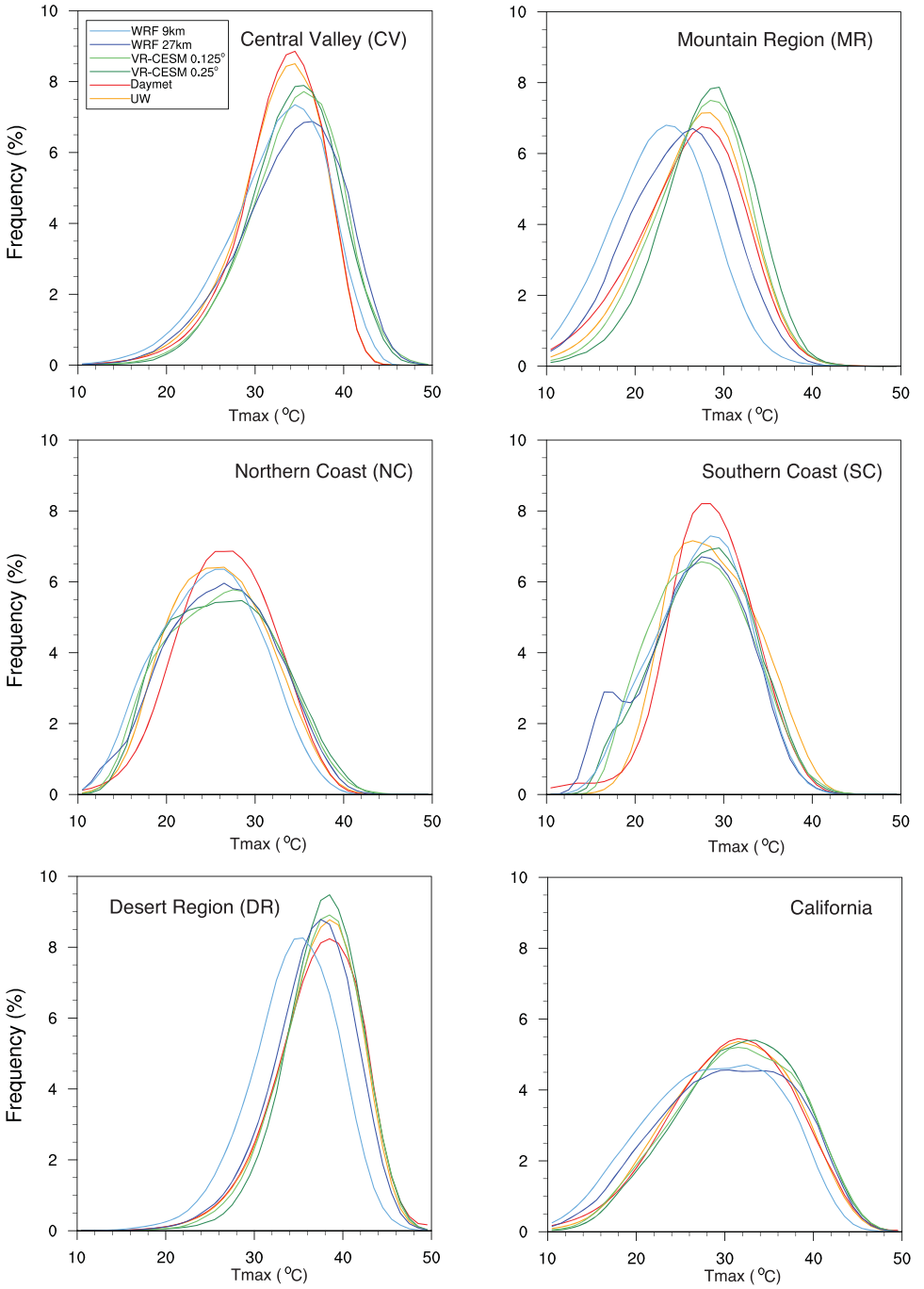

Figure 8. Frequency distribution of JJA daily T_{max} over the simulation period 1980–2005.

3.2. Precipitation

California's Mediterranean climate is associated with heavy precipitation in winter months and drier conditions in summertime. Agricultural and urban water use in California thus depends on accumulation of wintertime precipitation, which accounts for approximately half of total annual average precipitation as we calculated.

The long-term average climatology of DJF and annual daily Pr over 26 years from simulations and reference data sets (including PRISM and NARR) is depicted in Figure 9. Other reference data sets match closely with PRISM. Statistical quantities for precipitation over California are given in Table 6. We can see that

Table 5. The First Four Moments of the JJA T_{max} Frequency in Each Climate Division[a]

	CV				MR			
	Avg	Var	Skew	Kurt	Avg	Var	Skew	Kurt
UW	32.6	24.8	−0.8	0.9	26.7	33.2	−0.4	0.3
Daymet	32.7	23.5	−0.9	1.5	25.9	39.3	−0.5	0.5
VR-CESM 0.25°	34.1	26.2	−0.4	0.2	28.1	27.6	−0.4	0.3
VR-CESM 0.125°	34.3	28.5	−0.5	0.4	27.2	30.0	−0.4	0.3
WRF 27 km	33.9	34.8	−0.5	0.2	24.9	34.8	−0.3	0.0
WRF 9 km	32.4	33.1	−0.7	0.6	22.4	38.5	−0.5	0.6

	NC				SC				DR			
	Avg	Var	Skew	Kurt	Avg	Var	Skew	Kurt	Avg	Var	Skew	Kurt
UW	25.9	30.4	0.1	−0.5	25.9	30.4	0.1	−0.5	37.0	22.9	−0.6	0.7
Daymet	26.5	30.1	−0.3	0.4	26.5	30.1	−0.3	0.4	37.0	24.3	−0.6	0.6
VR-CESM 0.25°	26.4	37.4	0.1	−0.7	26.4	37.4	0.1	−0.7	37.6	19.0	−0.5	0.8
VR-CESM 0.125°	26.3	37.4	0.1	−0.6	26.3	37.4	0.1	−0.6	37.3	21.3	−0.5	0.4
WRF 27 km	26.0	36.7	−0.1	−0.5	26.0	36.7	−0.1	−0.5	36.5	22.6	−0.6	0.5
WRF 9 km	24.9	32.6	0.0	−0.6	24.9	32.6	0.0	−0.6	34.4	24.4	−0.5	0.4

[a]Column titles refer to the Average (Avg), Variance (Var), Skewness (Skew), and Kurtosis (Kurt). *Notes*: If skew >0 [skew <0], the distribution trails off to the right [left]. If kurtosis >0 [<0], a sharper [flatter] peak compared to a normal distribution (leptokurtic and platykurtic, respectively) is expected.

precipitation is heavily influenced by orography, leading to most accumulation occurring along the NC and MR. As with temperature, the model results match the spatial patterns of the PRISM, with high spatial correlation coefficients ($>$0.94).

For DJF Pr, especially along the western edge of the Sierra Nevada and into the CV, VR-CESM overestimates total precipitation ($\sim$25%–35%) relative to PRISM (see MRD in Table 6), particularly for the coarser resolution (0.25°) simulation. This difference is statistically significant over the western edge of the Sierra Nevada compared to PRISM at the 95% level for VR-CESM 0.25°. VR-CESM 0.125° performs better and produces far more realistic (and less scale sensitive) precipitation over the Sierra Nevada with improved treatment of orographic effects. On the other hand, precipitation is slightly underestimated relative to PRISM along the NC (with a statistically significant difference), particularly near the Oregon border. There are also notable differences between WRF 27 km and WRF 9 km. For DJF Pr, WRF 27 km underestimates precipitation along the NC (by about 20%–30%) but fairly accurately captures precipitation in the CV; whereas WRF 9 km greatly overestimates precipitation (by about 65%–85%) along the NC and MR (see MRD in Table 6). Using Table 6 as a guide, VR-CESM 0.125° performs better than VR-CESM 0.25° and WRF 27 km with RMSD values around 1.2 mm/d over DJF. Since we expect most of this improvement is due to a better representation of topography at 0.125°, this result suggests that the default physical parameterization suite in CESM is fairly resolution insensitive. WRF 9 km is significantly different from PRISM over the MR and part of NC, and the potential reasons are discussed at the end of this section. The differences between WRF simulations suggest a strong resolution dependence in the underlying microphysics, likely in part since WSM6 has been observed to produce excess graupel [*Jankov et al*., 2009]. However, the resolution dependence could also manifest in the boundary layer and convection schemes, which remains a topic for future investigation.

Interannual variability of precipitation was calculated for the models and PRISM using the standard deviation of annual and DJF precipitation and depicted in Figure 10. In general, precipitation variability exhibits a similar pattern to the precipitation intensity. The spatial pattern of variability agrees well between models and PRISM, with the closest match provided by VR-CESM 0.125° and WRF 27 km. Standard deviation is $\sim$50% higher for WRF 9 km, consistent with overestimated precipitation intensity. VR-CESM 0.25° also tends to overestimate variability in the southern Sierra Nevada, likely due to over enhanced orographic uplift from the relatively coarse topography (relative to 0.125°). Comparing with all the gridded observations, RMSD values are $\sim$0.7–0.9 mm/d for VR-CESM, $\sim$0.5–0.7 mm/d for WRF 27 km, and $\sim$1.7–2.0 mm/d for WRF 9 km.

The annual cycle of precipitation averaged over each month and region for the models and reference data sets (taking PRISM and NARR as representative of all data sets) is presented in Figure 11. The 95% confidence intervals of UW and PRISM are also depicted; differences between models and reference data sets

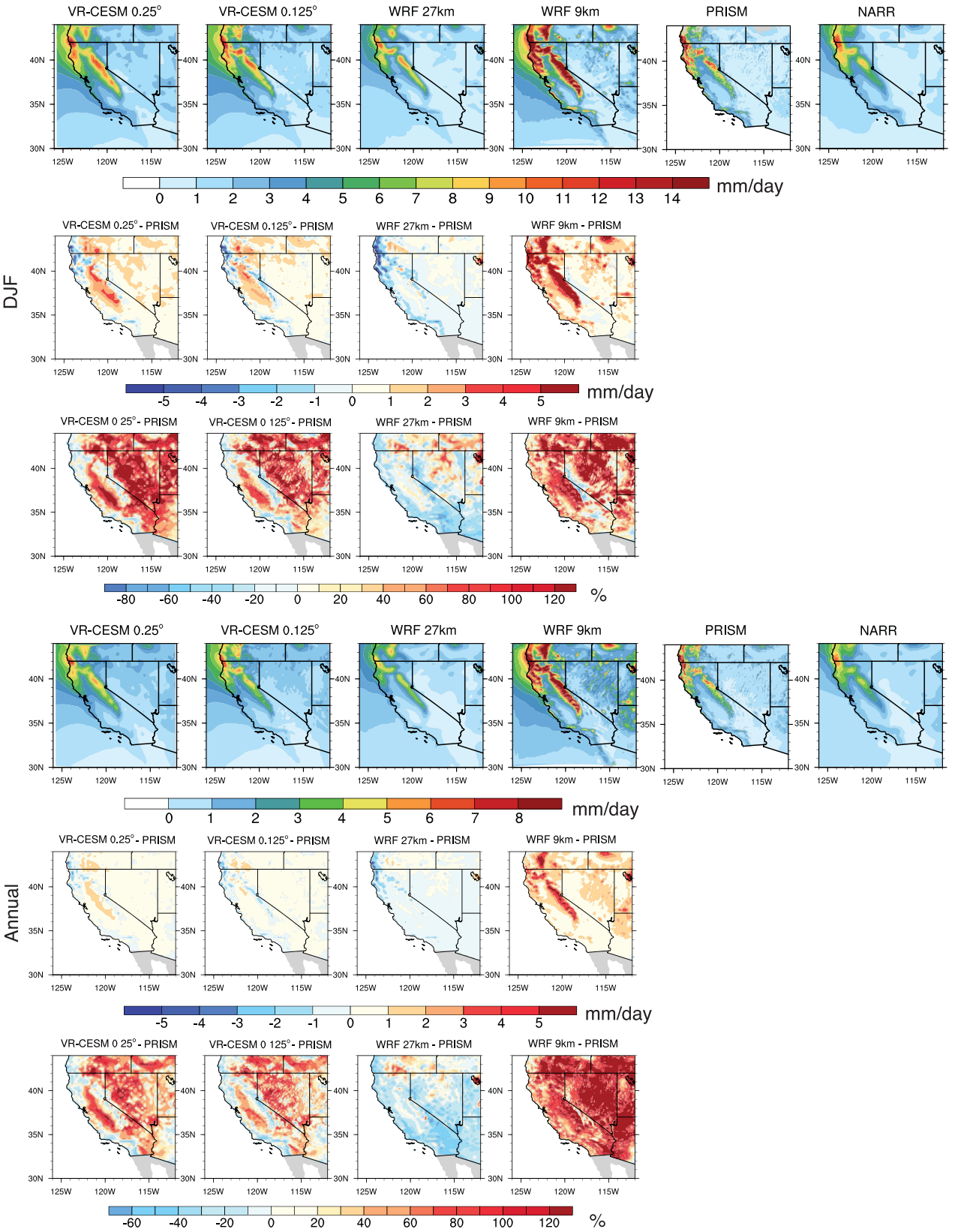

Figure 9. Annual and DJF precipitation from model results and reference data sets, absolute/relative differences between model results and PRISM.

Table 6. RMSD (mm/d), MSD (mm/d), MRD, Spatial Correlation (Corr) for Averaged Precipitation Over California

	CPC				UW			
Annual	RMSD	MSD	MRD	Corr	RMSD	MSD	MRD	Corr
VR-CESM 0.25°	0.61	0.39	0.30	0.98	0.62	0.29	0.29	0.96
VR-CESM 0.125°	0.47	0.21	0.24	0.98	0.53	0.12	0.24	0.97
WRF 27 km	0.42	−0.21	0.21	0.97	0.58	−0.31	0.24	0.97
WRF 9 km	2.23	1.49	0.97	0.95	2.05	1.39	0.85	0.96
Uniform CESM 1°	1.97	−1.57	0.99	0.94	2.31	−1.70	0.99	0.91
	PRISM				Daymet			
	RMSD	MSD	MRD	Corr	RMSD	MSD	MRD	Corr
VR-CESM 0.25°	0.72	0.20	0.31	0.95	0.57	0.19	0.25	0.97
VR-CESM 0.125°	0.62	0.05	0.26	0.96	0.50	0.03	0.22	0.97
WRF 27 km	0.77	−0.40	0.27	0.96	0.65	−0.41	0.27	0.97
WRF 9 km	1.89	1.32	0.78	0.97	2.01	1.31	0.76	0.96
Uniform CESM 1°	2.53	−1.83	0.99	0.90	2.31	−1.80	0.99	0.93
	CPC				UW			
DJF	RMSD	MSD	MRD	Corr	RMSD	MSD	MRD	Corr
VR-CESM 0.25°	1.49	0.99	0.36	0.97	1.45	0.67	0.33	0.95
VR-CESM 0.125°	1.19	0.64	0.29	0.97	1.23	0.35	0.27	0.96
WRF 27 km	0.89	−0.38	0.21	0.97	1.29	−0.69	0.26	0.96
WRF 9 km	4.26	2.61	0.86	0.95	3.84	2.32	0.70	0.95
Uniform CESM 1°	3.97	−3.12	0.99	0.93	4.80	−3.50	0.99	0.90
	PRISM				Daymet			
	RMSD	MSD	MRD	Corr	RMSD	MSD	MRD	Corr
VR-CESM 0.25°	1.65	0.58	0.35	0.94	1.35	0.51	0.28	0.96
VR-CESM 0.125°	1.40	0.29	0.29	0.95	1.17	0.21	0.25	0.96
WRF 27 km	1.55	−0.79	0.28	0.96	1.35	−0.85	0.28	0.96
WRF 9 km	3.57	2.26	0.66	0.96	3.80	2.18	0.65	0.95
Uniform CESM 1°	5.07	−3.65	0.99	0.90	4.69	−3.65	0.99	0.93

are statistically significant when simulation results appear outside the highlighted region. In general, the overall monthly climatology is consistent between models and reference data sets, with highest precipitation values occurring over winter and lowest values over summer. Nonetheless, the largest deviations occur during the winter season. WRF 27 km is drier than PRISM and UW with relative differences ranging from ∼10% to 40%, whereas WRF 9 km is far wetter with relative differences reaching up to 40%–80% over these five divisions. VR-CESM tracks well with observed precipitation with ∼10%–20% relative difference everywhere except in the CV, where precipitation is overestimated in the rainy seasons by about 70%–80%. From the MWW test, VR-CESM and WRF 27 km are not significantly different from reference data sets in most divisions, except over the CV in late winter to spring for VR-CESM 0.25°, and the NC winter and spring, and DR's winter for WRF 27 km. The magnitude of precipitation in WRF 9 km is significantly different from the reference data sets over most divisions, except DR and SC's winter and spring. Nonetheless, the strong seasonal dependence on precipitation is apparent with extremely dry conditions during summer months. A slight increase in summertime precipitation is apparent in the DR, indicating the North American monsoon. We also observe that the peak month for precipitation tends to occur earlier in VR-CESM, particularly at 0.125°, compared with the reference. VR-CESM also exhibits some unexpected jaggedness (particularly December for VR-CESM 0.25° and February for VR-CESM 0.125°), likely due to an issue with capturing the seasonality of moisture transport over the Pacific. This issue being driven by variability outside the high-resolution domain seems corroborated by the observation that WRF correlates strongly with the reference data sets (even though the reported magnitude is incorrect).

The monthly cycle of sample standard deviation is depicted in Figure 7 for California (results are similar for subregions when renormalized by the mean precipitation). Again, the 95% confidence interval from the chi-square test is depicted from PRISM to identify statistically significant differences (although this test should not be employed for nonnormal samples, such as monthly average precipitation, we have confirmed similar

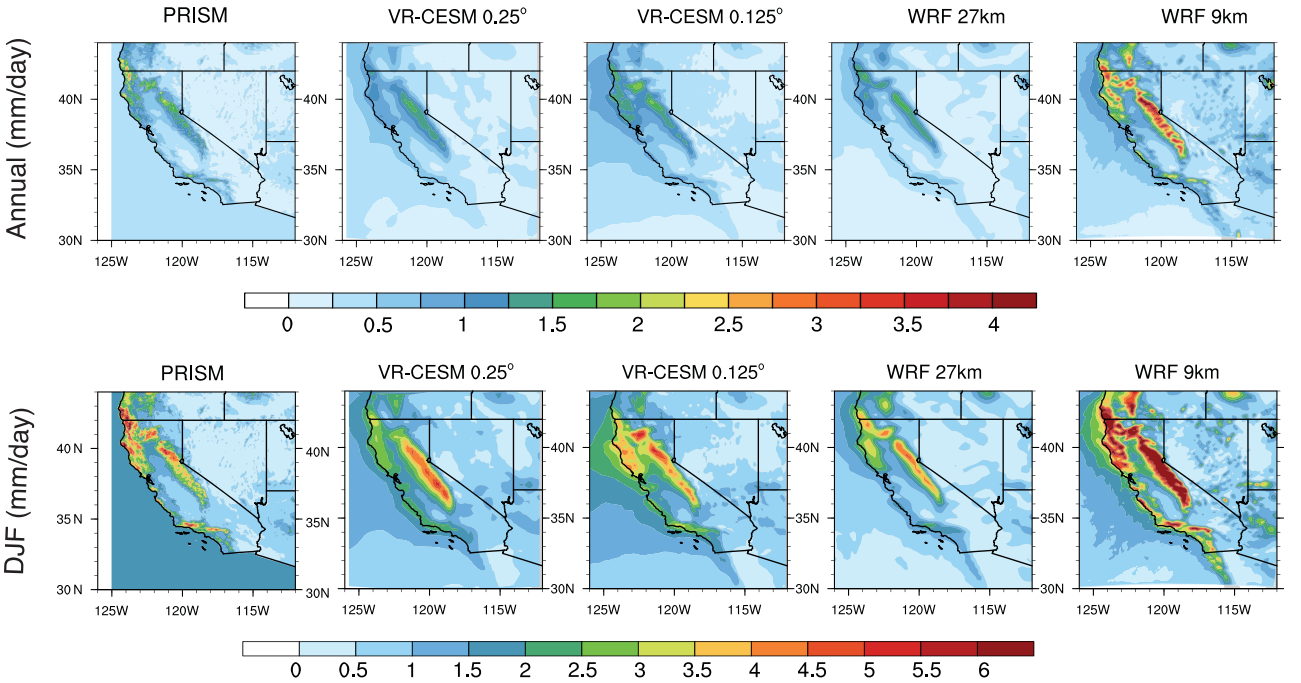

Figure 10. Sample standard deviation of annual and DJF precipitation from models and PRISM.

results under Levene's test). The variability in observations has a similar monthly trend as precipitation rate, with overall values from 0 to 4 mm/d. Generally, higher interannual variability occurs over locations with higher mean precipitation (see Figure 11), also observed by previous studies [for example, *Duffy et al*., 2006]. Compared with observations, VR-CESM exhibited ∼1 mm/d larger variability in the rainy season with RMSDs ranging from ∼0.2 to 0.9 mm/d (see Table 4). WRF 9 km also showed enhanced variability, especially during the wintertime (∼1.5 mm/d more), with significant difference from references. WRF 27 km captured the interannual variability quite well with only minor underestimation except the coastal regions, with RMSDs around 0.1–0.7 mm/d. The primary driver for the interannual variability of precipitation over California is the El Niño-Southern Oscillation (ENSO), which impacts the moisture flux transport to this region [*Cayan et al*., 1998, 1999; *Leung et al*., 2003b].

The frequency distribution of DJF Pr has been constructed from rainy days ($Pr \geq 0.1$ mm/d) for simulations and reference data sets and is depicted in Figure 12. Since the frequency of precipitation is very similar across all reference data sets, only UW and CPC are included. Generally, VR-CESM matches closely with observations everywhere except in the CV. In the CV, WRF 27 km appears to better capture high-intensity precipitation events but performs poorly on low-intensity events ($Pr < 20$ mm/d). The underestimation of rainfall frequency in WRF 27 km appears consistent across divisions. WRF 9 km produces a significantly better treatment of low-intensity events but greatly overestimates the frequency of high-intensity events ($Pr > 20$ mm/d). For strong precipitation events, VR-CESM matches closely to observations everywhere except the CV.

The overestimation of precipitation for WRF at high resolution has also been found in previous studies. Although not as pronounced as WRF 9 km here, *Caldwell et al*. [2009] demonstrated that WRF at 12 km largely overestimated the precipitation over California's mountainous regions (however, this paper did employ a different set of parameterizations and had a different spatial extent of mountain region). Further discussion can be found in former studies that employ different microphysics schemes (and so produce a wide range of precipitation magnitudes) [*Jankov et al*., 2005; *Chin et al*., 2010; *Caldwell*, 2010]. However, *Caldwell et al*. [2009] also argued that the bias comes from a variety of sources, rather than simply different choices of subgrid-scale parameterizations. The exact cause of this overprediction has yet to be identified in the literature and a comprehensive analysis of the cause of these errors is beyond the scope of this paper.

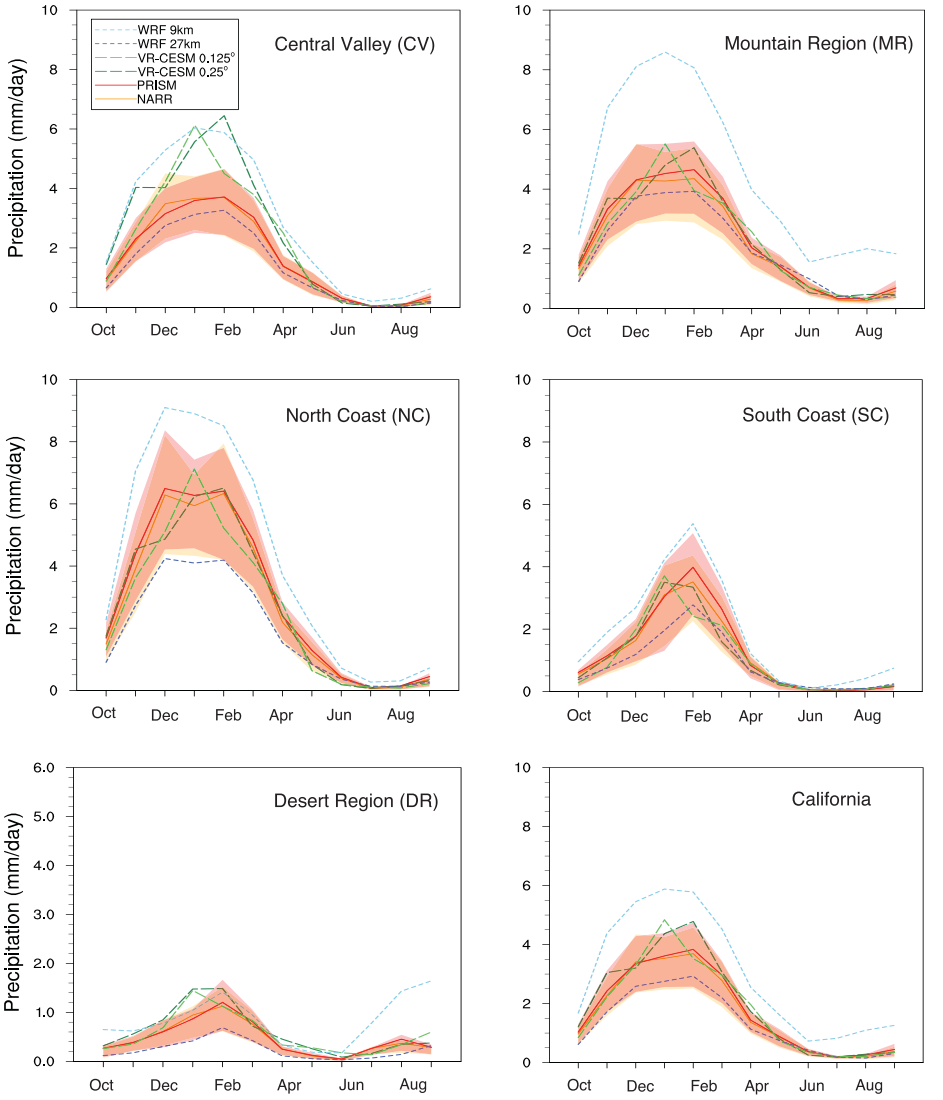

Figure 11. As Figure 6, but for monthly average total precipitation. The shading refers to the 95% confidence interval of PRISM and UW.

3.3. Overall Performance and Extreme Events

A simple schematic summary is given in Table 7 indicating observed biases from VR-CESM and WRF by region relative to PRISM. As mentioned earlier, over the coastal regions (especially NC) the observational data sets show significant uncertainty (see Table 2) that must be taken into account. In general, both VR-CESM and WRF correlate well with observations. WRF is better at capturing T_{min}, but VR-CESM provides a better estimate of T_{max}. WRF 9 km grossly overestimate DJF precipitation, with values nearly 2 times larger than observations. Overall, these observations indicate VR-CESM provides a competitive representation of the regional climatology over California with simulation biases that are comparable to WRF. Across resolutions, there is a small but clear improvement in using VR-CESM 0.125° compared to 0.25° for simulating T_{max} and Pr.

We now briefly address the behavior of VR-CESM 0.125° and WRF 9 km for simulating climatological extremes. Figure 13 depicts the spatial distribution of average number of days per year where T_{max} exceeds 35°, referred to as extreme heat days, and the average number of days per year where $Pr > 20$ mm/d, referred to as extreme precipitation days. The spatial patterns associated with these extremes match closely with simulated T_{max} from Figure 4, for extreme heat days, and simulated DJF precipitation from Figure 9, for extreme precipitation days. Consequently, we anticipate that improvements in the model's treatment of T_{max} and Pr will directly impact the capability of these models to simulate corresponding extremes.

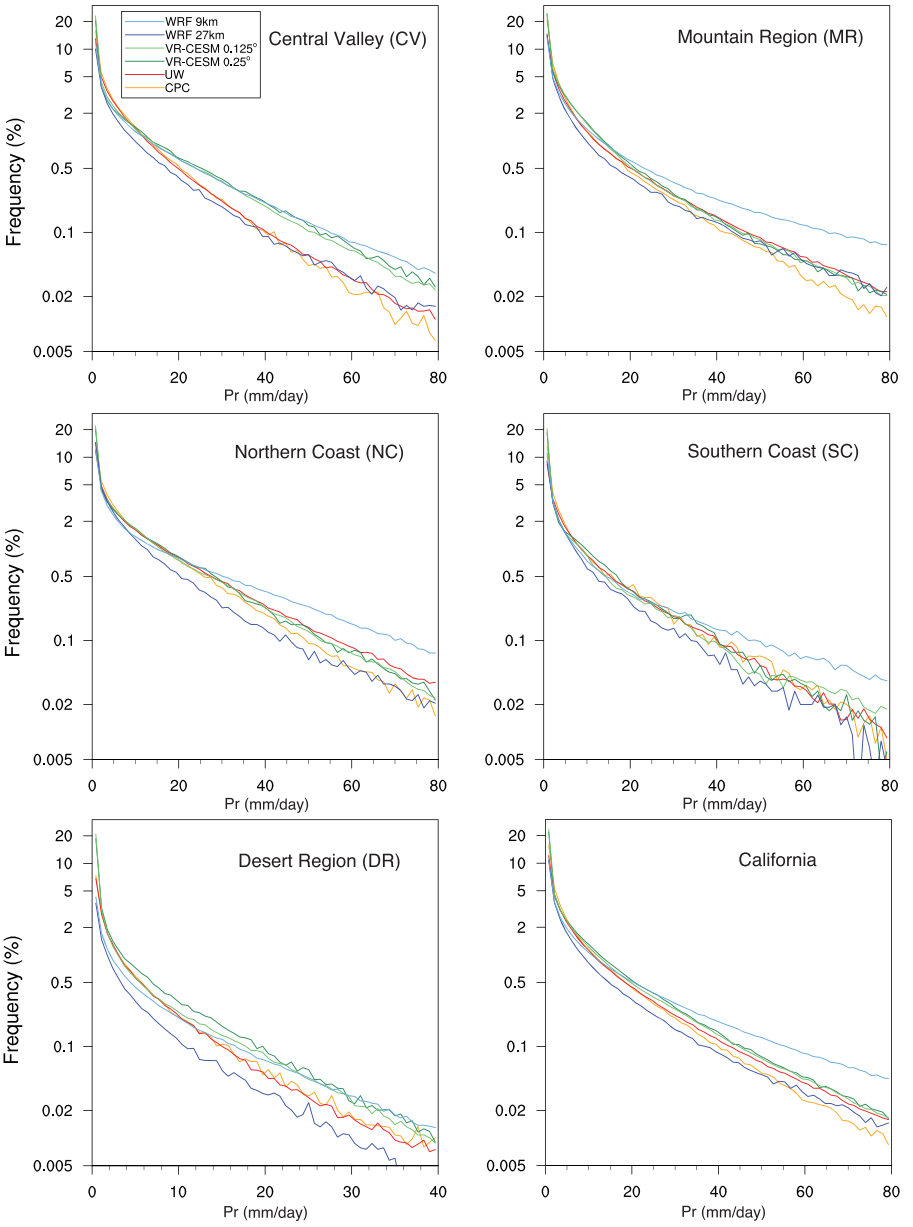

Figure 12. As Figure 8, but for DJF rainy days (Pr $\geq$ 0.1 mm/d) (note that the vertical scale is logarithmic).

4. Discussion and Summary

The need for high-resolution model data to address regional climate change and extreme events has motivated the development of new modeling tools. To support this work, this study investigated the variable-resolution Community Earth System Model (VR-CESM) for two-way dynamically downscaled climate modeling. VR-CESM was evaluated for modeling California's unique regional climate and compared against gridded observational data sets, reanalysis data, and the WRF model (forced with ERA-Interim data at lateral boundaries).

Based on 26 years of high-resolution historical climate simulations (1980–2005), we analyzed the mean climatology of California across its climate divisions in terms of both near-surface temperature and precipitation. Generally, when compared with gridded observational data sets, both VR-CESM and WRF adequately represented regional climatological patterns with high spatial correlations (>0.94). Uncertainty between reference data sets is apparent and is statistically significant over some climate divisions, making it necessary to utilize

Table 7. A Summary of the Biases in VR-CESMs and WRF, Compared to PRISM, for JJA T_{max}, JJA T_{min}, and DJF Pr in Each Region[a]

	VR-CESM 0.25°[b]			VR-CESM 0.125°[b]		
	T_{max} (°C)	T_{min} (°C)	Pr (%)	T_{max} (°C)	T_{min} (°C)	Pr (%)
CV	*2–3*	*2–3*	*70–100*	*2–3*	*2–3*	*30–60*
MR	*2–3*	*2–4*		*2*	*2–3*	
SC	**2**	*2–3*		**2**	*2–3*	
NC	**2–3**			**2–3**		
DR		*2–4*	*60*		*2–4*	*30*

	WRF 27 km[c]			WRF 9 km[c]	
	T_{max} (°C)	T_{min} (°C)	Pr (%)	T_{min} (°C)	Pr (%)
CV	*2–3*	**1**			*50–70*
MR	**2**	*2*		*2*	*70–100*
SC	**2**	*1*	**20–30**	*1*	*30*
NC	**2–4**		**20**	*1*	*30–60*
DR			**20–40**	*2*	

	WRF 27 km[c]			WRF 9 km[c]	
	T_{max} (°C)	T_{min} (°C)	Pr (%)	T_{min} (°C)	Pr (%)
CV	*1–2*				
MR	**3–4**				
SC	**2**				
NC	**2–4**				
DR	**2–3**				

[a]Italic (bold) entries indicate positive (negative) bias. Underlined entries indicate the most significant differences. Empty cells indicate no statistically significant difference.

[b]*Notes*: Over California, VR-CESM correctly captures the spatial interannual standard deviation of seasonal temperature and precipitation and interannual variability in monthly average T_{avg} and Pr (in both cases finer resolution performs better). In VR-CESM, the peak month for precipitation tends to occur earlier than in observations.

[c]*Notes*: Over California, WRF 27 km correctly captures the spatial interannual standard deviation of temperature and precipitation. WRF 27 km can also reproduce the monthly cycle of T_{avg}, and interannual variability of T_{avg} and Pr (better than VR-CESM).

more than one high-quality observational product in the model evaluation. Overall, we found that VR-CESM showed comparable performance to WRF for regional climate modeling at spatial resolutions of 10–30 km.

Simulated temperature was assessed in terms of the mean climatology of T_{min}, T_{max}, and T_{avg} and interannual monthly averaged variability of T_{avg}. Deviations between the models and the reference data sets were

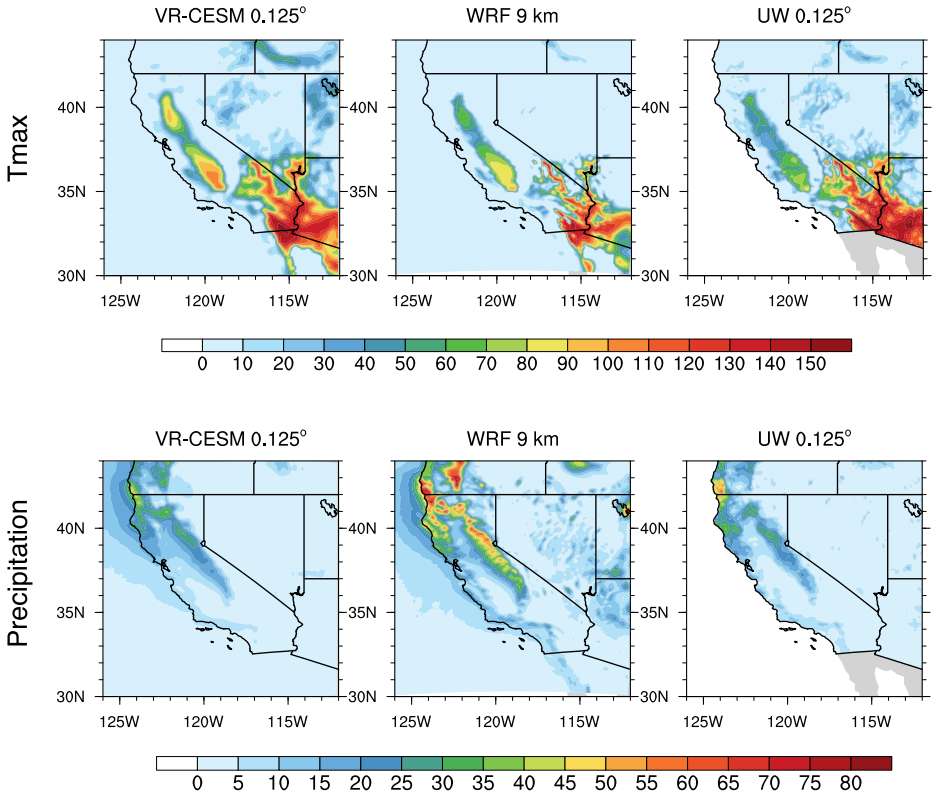

Figure 13. Number of days per year with (top) $T_{max} > 35$°C and (bottom) Pr > 20 mm/d in VR-CESM 0.125°, WRF 9 km and UW over the simulation period 1980–2005.

apparent, but their character differed between VR-CESM and WRF. During the summer period, VR-CESM produced a 2–3°C warmer climate than observations, especially in the CV. On the other hand, WRF exhibited a colder (∼2°C) T_{max} over most divisions (except the CV) but was only a little warmer in T_{min}. Overall, VR-CESM was more accurate in reproducing mean climatology of T_{max}, whereas WRF was better at modeling T_{min} and T_{avg}. WRF modeled the annual cycle of T_{avg} better than VR-CESM with about a 1°C overall underestimation. VR-CESM overestimated T_{avg} by 2°C over the summer season and underestimated T_{avg} by 2°C over the winter season, indicating a larger annual temperature range over most divisions. Higher-resolution (0.125°) VR-CESM captures the spatial pattern of annual variability for near-surface temperature pattern shown in PRISM. Both WRF and VR-CESM well represent variability in monthly average T_{avg} over each climate division, except for the WRF 9 km in January and February where variability was greatly overestimated.

Temperatures were further investigated in terms of the climatology of JJA T_{max}, due to its relevance to summertime heat waves. Both models successfully simulated the spatial character of JJA T_{max}, although both also had an apparent warm bias over the CV. The failure to correctly capture CV T_{max} is likely caused in part by the lack of irrigation cooling over this division in both models. Future work will address this issue by applying irrigation model to VR-CESM so as to figure out the role irrigation plays in regulating T_{max} and its frequency distribution.

Precipitation was assessed in terms of mean climatology, interannual monthly averaged variability and frequency of precipitation intensity. In general, VR-CESM matched closely with PRISM everywhere except for an overestimation of DJF Pr (about 25%–35%) along the western flank of the Sierra Nevada and into the CV. Increasing the spatial resolution to 0.125° produced some reduction in this overestimation (about 10%) likely due to improved treatment of orographic effects. WRF 27 km underestimated DJF precipitation (by about 20%–30%) along the NC and MR (where almost all the precipitation appears), whereas WRF 9 km showed a large overestimation (about 65%–85%). The standard deviation of precipitation ranged from 0 to 6 mm/d, with generally higher interannual variability over locations of higher mean precipitation. When assessing the frequency of strong precipitation events, VR-CESM matched closely to the UW data set everywhere except the CV.

Higher-resolution (0.125°) VR-CESM did produce better results when assessing JJA T_{max} and precipitation (along with their variability), compared with the coarser resolution run. However, the improvements were not statistically significant over most of the study area. The largest improvement at higher resolution was in the spatial character of precipitation, driven primarily with a better representation of the underlying topography. Notably, this result highlights the relative insensitivity to resolution in VR-CESM's physical parameterizations. This may be an advantageous result for multiscale modelers interested in climate applications. Correctly simulating precipitation is vital to properly representing snowpack, which is of critical importance to water availability in the western United States [*Bales et al*., 2006; *Wise*, 2012; *Rhoades et al*., 2015]. Decreased scale sensitivity implies the result will be more independent of the choice of grid resolution. However, since the range of scales in this investigation is small (∼28 km to ∼14 km), we do not discount sensitivity over a wider range of scales [*Wehner et al*., 2010; *Rauscher et al*., 2010]. Notably, for both regional and global models, resolution effects do not typically have a linear dependency [e.g., *Hughes et al*., 2014; *Wehner et al*., 2014].

For WRF, when resolution is increased to 9 km, the model produces vastly overestimated precipitation, as previous studies have also found when using RCMs for fine-scale regional simulations. Although the convective parameterization was not disabled (as is suggested for some models below 10 km resolution), the effect of this change is minor since almost all of the precipitation comes from resolved (large-scale) condensation (not shown). In this sense, precipitation modeling bias of WRF is more strongly related with resolved-scale processes and the choice of microphysics scheme plays a major role, motivating the need for more work on scale-aware parameterizations [*O'Brien et al*., 2013].

Regarding computational cost, we note that a direct comparison between VR-CESM and WRF is somewhat misleading, due to widely disparate configurations of each model (for instance, differences in dynamical core, parameterization suite, optimization strategy, and output variables). Nonetheless, for our simulations, we report core hours per grid point, where the total number of grid points is equal to the number of atmospheric columns multiplied by number of model levels. VR-CESM was configured with 30 model levels and 75,062 (101,954) columns on the 0.25° (0.125°) mesh, whereas WRF was configured with 41 model levels

and 13,200 (39,172) columns for the 27 km (9 km) simulations. The high-resolution region represented approximately 1/3 and 1/2 of all grid points in VR-CESM at 0.25° and 0.125°, respectively. On the Yellowstone cluster, we observed that VR-CESM simulations at 0.25° (0.125°) required 0.0043 (0.0037) core hours per grid point per simulated year, compared with 0.0011 (0.0027) core hours of that with WRF 27 km (WRF 9 km). In our experiments, VR-CESM demonstrated effectively linear scalability in the number of elements simulated.

In summary, VR-CESM demonstrated competitive utility for studying high-resolution regional climatology when compared to a regional climate model (WRF). Compared to regional models, variable-resolution models are more suitable for regional climate studies where nonlocal processes are a major influence, including two-way interactions at the nest boundary and potential upstream impacts [*Sakaguchi et al*., 2015]. Variable-resolution models are also useful for assessing and tuning resolution dependence of physical parameterizations in global models and are also valuable for short-term weather prediction [*Zarzycki and Jablonowski*, 2015]. On the other hand, RCMs tend to have more subgrid parameterization choices that can be tailored for particular studies [e.g., *Cassano et al*., 2011] and tend to be more efficient, as computational expense can be precisely targeted. Deviations exhibited within these models are not indicative of deep underlying problems with the model formulation, but one should nonetheless be aware of these biases when using these models for climate studies. This study suggests that VRGCMs are, in general, useful tools for assessing climate change over the coming century. As the need for assessments of regional climate change increases, alternative modeling strategies, including VRGCMs will be needed to improve our understanding of the effects of fine-scale processes representation in regional climate regulation. Future work will focus on the capability of the variable-resolution system to correctly capture the features of discrete, extreme heat and precipitation events.

Acknowledgments

The authors thank Travis O'Brien for the many useful conversations on climate model assessment. We also want to thank Xue Meng Chen for her assistance in performing the WRF simulations. We acknowledge the work done to create the following data sets used in this study including PRISM, UW, Daymet, NARR, and CPC (provided by the NOAA/OAR/ESRL PSD, Boulder, Colorado, USA, from their Web site at http://www.esrl.noaa.gov/psd/). The simulation data used are available by request at xyhuang@ucdavis.edu. This project is supported in part by the University of California, Davis and by the Department of Energy "Multiscale Methods for Accurate, Efficient, and Scale-Aware Models of the Earth System" program. Support also came from the USDA National Institute of Food and Agriculture, California Agricultural Experiment Station Hatch project CA-D-LAW-2203-H.

References

Abatzoglou, J. T., K. T. Redmond, and L. M. Edwards (2009), Classification of regional climate variability in the state of California, *J. Appl. Meteorol. Climatol.*, *48*(8), 1527–1541.

Bales, R. C., N. P. Molotch, T. H. Painter, M. D. Dettinger, R. Rice, and J. Dozier (2006), Mountain hydrology of the western United States, *Water Resour. Res.*, *42*, W08432, doi:10.1029/2005WR004387.

Bonfils, C., and D. Lobell (2007), Empirical evidence for a recent slowdown in irrigation-induced cooling, *Proc. Natl. Acad. Sci. U. S. A.*, *104*(34), 13,582–13,587.

Bukovsky, M. S., and D. J. Karoly (2007), A brief evaluation of precipitation from the North American Regional Reanalysis, *J. Hydrometeorol.*, *8*(4), 837–846.

Bukovsky, M. S., and D. J. Karoly (2009), Precipitation simulations using WRF as a nested regional climate model, *J. Appl. Meteorol. Climatol.*, *48*(10), 2152–2159.

Caldwell, P. (2010), California wintertime precipitation bias in regional and global climate models, *J. Appl. Meteorol. Climatol.*, *49*(10), 2147–2158.

Caldwell, P., H.-N. S. Chin, D. C. Bader, and G. Bala (2009), Evaluation of a WRF dynamical downscaling simulation over California, *Clim. Change*, *95*(3–4), 499–521.

Cassano, J. J., M. E. Higgins, and M. W. Seefeldt (2011), Performance of the weather research and forecasting model for month-long pan-arctic simulations, *Mon. Weather Rev.*, *139*(11), 3469–3488.

Cayan, D. R., M. D. Dettinger, H. F. Diaz, and N. E. Graham (1998), Decadal variability of precipitation over western North America, *J. Clim.*, *11*(12), 3148–3166.

Cayan, D. R., K. T. Redmond, and L. G. Riddle (1999), ENSO and hydrologic extremes in the western United States, *J. Clim.*, *12*(9), 2881–2893.

Cayan, D. R., A. L. Luers, G. Franco, M. Hanemann, B. Croes, and E. Vine (2008), Overview of the California climate change scenarios project, *Clim. Change*, *87*(1), 1–6.

Chen, F., and J. Dudhia (2001), Coupling an advanced land surface-hydrology model with the Penn State-NCAR MM5 modeling system. Part I: Model implementation and sensitivity, *Mon. Weather Rev.*, *129*(4), 569–585.

Chin, H.-N. S., P. M. Caldwell, and D. C. Bader (2010), Preliminary study of California wintertime model wet bias, *Mon. Weather Rev.*, *138*(9), 3556–3571.

Christensen, et al. (2007), Regional climate projections, in *Climate Change, 2007: The Physical Science Basis. Contribution of Working Group I to the Fourth Assessment Report of the Intergovernmental Panel on Climate Change*, chap. 11, pp. 847–940, Univ. Press, Cambridge, U. K.

Collins, W. D., et al. (2004), Description of the NCAR Community Atmosphere Model (CAM 3.0), *Tech. Rep. NCAR/TN-464+ STR*, Nat. Cent. Atmos. Res., Boulder, Colo.

Daly, C., M. Halbleib, J. I. Smith, W. P. Gibson, M. K. Doggett, G. H. Taylor, J. Curtis, and P. P. Pasteris (2008), Physiographically sensitive mapping of climatological temperature and precipitation across the Conterminous United States, *Int. J. Climatol.*, *28*(15), 2031–2064.

Dee, D., et al. (2011), The ERA-Interim reanalysis: Configuration and performance of the data assimilation system, *Q. J. R. Meteorol. Soc.*, *137*(656), 553–597.

Dennis, J., J. Edwards, K. J. Evans, O. Guba, P. H. Lauritzen, A. A. Mirin, A. St-Cyr, M. A. Taylor, and P. H. Worley (2012), CAM-SE: A scalable spectral element dynamical core for the Community Atmosphere Model, *Int. J. High Performance Comput. Appl.*, *26*(1), 74–89.

Dinse, K. (2009), Climate variability and climate change: What is the difference, in *Book Climate Variability and Climate Change: What is the Difference*, Michigan Sea Grant, Global Change Research Program.

Duffy, P., R. Arritt, J. Coquard, W. Gutowski, J. Han, J. Iorio, J. Kim, L.-R. Leung, J. Roads, and E. Zeledon (2006), Simulations of present and future climates in the western United States with four nested regional climate models, *J. Clim.*, *19*(6), 873–895.

Fox-Rabinovitz, M., J. Côté, B. Dugas, M. Déqué, and J. L. McGregor (2006), Variable resolution general circulation models: Stretched-grid model intercomparison project (SGMIP), *J. Geophys. Res.*, *111*, D16104, doi:10.1029/2005JD006520.
Fox-Rabinovitz, M. S., G. L. Stenchikov, M. J. Suarez, and L. L. Takacs (1997), A finite-difference GCM dynamical core with a variable-resolution stretched grid, *Mon. Weather Rev.*, *125*(11), 2943–2968.
Gates, W. L. (1992), AMIP: The Atmospheric Model Intercomparison Project, *Bull. Am. Meteorol. Soc.*, *73*, 1962–1970.
Gettelman, A., H. Morrison, and S. J. Ghan (2008), A new two-moment bulk stratiform cloud microphysics scheme in the Community Atmosphere Model, version 3 (CAM3). Part II: Single-column and global results, *J. Clim.*, *21*(15), 3660–3679.
Guba, O., M. A. Taylor, P. A. Ullrich, J. R. Overvelt, and M. N. Levy (2014), The spectral element method on variable resolution grids: Evaluating grid sensitivity and resolution-aware numerical viscosity, *Geosci. Model Dev.*, *7*, 2803–2816, doi:10.5194/gmd-7-2803-2014.
Hamlet, A. F., and D. P. Lettenmaier (2005), Production of temporally consistent gridded precipitation and temperature fields for the continental United States, *J. Hydrometeorol.*, *6*(3), 330–336.
Hayhoe, K., et al. (2004), Emissions pathways, climate change, and impacts on California, *Proc. Natl. Acad. Sci. U. S. A.*, *101*(34), 12,422–12,427.
Hong, S.-Y., and J.-O. J. Lim (2006), The WRF single-moment 6-class microphysics scheme (WSM6), *Asia-Pacific J. Atmos. Sci.*, *42*(2), 129–151.
Hong, S.-Y., Y. Noh, and J. Dudhia (2006), A new vertical diffusion package with an explicit treatment of entrainment processes, *Mon. Weather Rev.*, *134*(9), 2318–2341.
Hughes, M., K. M. Mahoney, P. J. Neiman, B. J. Moore, M. Alexander, and F. M. Ralph (2014), The landfall and inland penetration of a flood-producing atmospheric river in Arizona. Part II: Sensitivity of modeled precipitation to terrain height and atmospheric river orientation, *J. Hydrometeorol.*, *15*(5), 1954–1974.
Hurrell, J. W., J. J. Hack, D. Shea, J. M. Caron, and J. Rosinski (2008), A new sea surface temperature and sea ice boundary dataset for the Community Atmosphere Model, *J. Clim.*, *21*(19), 5145–5153.
Hurrell, J. W., et al. (2013), The Community Earth System Model: A framework for collaborative research, *Bull. Am. Meteorol. Soc.*, *94*(9), 1339–1360.
Jankov, I., W. A. Gallus Jr., M. Segal, B. Shaw, and S. E. Koch (2005), The impact of different WRF model physical parameterizations and their interactions on warm season MCS rainfall, *Weather Forecasting*, *20*(6), 1048–1060.
Jankov, I., J.-W. Bao, P. J. Neiman, P. J. Schultz, H. Yuan, and A. B. White (2009), Evaluation and comparison of microphysical algorithms in ARW-WRF model simulations of atmospheric river events affecting the California coast, *J. Hydrometeorol.*, *10*(4), 847–870.
Kain, J. S. (2004), The Kain-Fritsch convective parameterization: An update, *J. Appl. Meteorol.*, *43*(1), 170–181.
Kanamitsu, M., and H. Kanamaru (2007), Fifty-seven-year California Reanalysis Downscaling at 10 km (CaRD10). Part I: System detail and validation with observations, *J. Clim.*, *20*(22), 5553–5571.
Kueppers, L. M., M. A. Snyder, and L. C. Sloan (2007), Irrigation cooling effect: Regional climate forcing by land-use change, *Geophys. Res. Lett.*, *34*, L03703, doi:10.1029/2006GL028679.
Laprise, R. (2008), Regional climate modelling, *J. Comput. Phys.*, *227*(7), 3641–3666.
Laprise, R., R. De Elia, D. Caya, S. Biner, P. Lucas-Picher, E. Diaconescu, M. Leduc, A. Alexandru, and L. Separovic (2008), Challenging some tenets of regional climate modelling, *Meteorol. Atmos. Phys.*, *100*(1–4), 3–22.
Leung, L. R., and Y. Qian (2009), Atmospheric rivers induced heavy precipitation and flooding in the western US simulated by the WRF regional climate model, *Geophys. Res. Lett.*, *36*, L03820, doi:10.1029/2008GL036445.
Leung, L. R., L. O. Mearns, F. Giorgi, and R. L. Wilby (2003a), Regional climate research: needs and opportunities, *Bull. Am. Meteorol. Soc.*, *84*(1), 89–95.
Leung, L. R., Y. Qian, X. Bian, and A. Hunt (2003b), Hydroclimate of the western United States based on observations and regional climate simulation of 1981–2000. Part II: Mesoscale ENSO anomalies, *J. Clim.*, *16*(12), 1912–1928.
Leung, L. R., Y. Qian, X. Bian, W. M. Washington, J. Han, and J. O. Roads (2004), Mid-century ensemble regional climate change scenarios for the western United States, *Clim. Change*, *62*(1–3), 75–113.
Liu, P., A. Tsimpidi, Y. Hu, B. Stone, A. Russell, and A. Nenes (2012), Differences between downscaling with spectral and grid nudging using WRF, *Atmos. Chem. Phys.*, *12*(8), 3601–3610.
Lo, J. C.-F., Z.-L. Yang, and R. A. Pielke (2008), Assessment of three dynamical climate downscaling methods using the Weather Research and Forecasting (WRF) model, *J. Geophys. Res.*, *113*, D09112, doi:10.1029/2007JD009216.
Maurer, E., A. Wood, J. Adam, D. Lettenmaier, and B. Nijssen (2002), A long-term hydrologically based dataset of land surface fluxes and states for the Conterminous United States, *J. Clim.*, *15*(22), 3237–3251.
McDonald, A. (2003), Transparent boundary conditions for the shallow-water equations: Testing in a nested environment, *Mon. Weather Rev.*, *131*(4), 698–705.
McGregor, J. L., and M. R. Dix (2008), An updated description of the conformal-cubic atmospheric model, in *High Resolution Numerical Modelling of the Atmosphere and Ocean*, pp. 51–75, Springer, Berlin, Germany.
Mearns, L. O., et al. (2012), The North American regional climate change assessment program: Overview of phase I results, *Bull. Am. Meteorol. Soc.*, *93*(9), 1337–1362.
Mesinger, F., and K. Veljovic (2013), Limited area NWP and regional climate modeling: A test of the relaxation vs Eta lateral boundary conditions, *Meteorol. Atmos. Phys.*, *119*(1–2), 1–16.
Mesinger, F., et al. (2006), North American Regional Reanalysis, *Bull. Am. Meteorol. Soc.*, *87*, 343–360.
Morrison, H., and A. Gettelman (2008), A new two-moment bulk stratiform cloud microphysics scheme in the Community Atmosphere Model, version 3 (CAM3). Part I: Description and numerical tests, *J. Clim.*, *21*(15), 3642–3659.
Neale, R. B., et al. (2010a), Description of the NCAR Community Atmosphere Model (CAM 5.0), *NCAR Tech. Note NCAR/TN-486+ STR*, Nat. Cent. Atmos. Res., Boulder, Colo.
Neale, R. B., C.-C. Chen, and A. Gettelman (2010b), Description of the NCAR Community Atmosphere Model (CAM 5.0), *NCAR Tech. Note NCAR/TN-486+STR*, Natl. Cent. Atmos. Res., Boulder, Colo.
O'Brien, T. A., et al. (2013), Observed scaling in clouds and precipitation and scale incognizance in regional to global atmospheric models, *J. Clim.*, *26*(23), 9313–9333.
Oleson, K., et al. (2010), Technical description of version 4.0 of the Community Land Model (CLM), *NCAR Tech. Note NCAR/TN-478+STR*, Natl. Cent. for Atmos. Res., Boulder, Colo., doi:10.5065/D6FB50WZ.
Pan, L.-L., S.-H. Chen, D. Cayan, M.-Y. Lin, Q. Hart, M.-H. Zhang, Y. Liu, and J. Wang (2011), Influences of climate change on California and Nevada regions revealed by a high-resolution dynamical downscaling study, *Clim. Dyn.*, *37*(9–10), 2005–2020.
Pierce, D. W., et al. (2013), Probabilistic estimates of future changes in California temperature and precipitation using statistical and dynamical downscaling, *Clim. Dyn.*, *40*(3–4), 839–856.

Rauscher, S. A., E. Coppola, C. Piani, and F. Giorgi (2010), Resolution effects on regional climate model simulations of seasonal precipitation over Europe, *Clim. Dyn.*, *35*(4), 685–711.
Rauscher, S. A., T. D. Ringler, W. C. Skamarock, and A. A. Mirin (2013), Exploring a global multiresolution modeling approach using aquaplanet simulations, *J. Clim.*, *26*(8), 2432–2452.
Rhoades, A. M., X. Huang, P. A. Ullrich, and C. M. Zarzycki (2015), Characterizing Sierra Nevada Snowpack using variable-resolution CESM, *J. Appl. Meteorol. Climatol.*, *55*, 173–196.
Ringler, T., L. Ju, and M. Gunzburger (2008), A multiresolution method for climate system modeling: Application of spherical centroidal Voronoi tessellations, *Ocean Dyn.*, *58*(5–6), 475–498.
Sakaguchi, K., L. R. Leung, C. Zhao, Q. Yang, J. Lu, S. Hagos, S. A. Rauscher, L. Dong, T. D. Ringler, and P. H. Lauritzen (2015), Exploring a multi-resolution approach using AMIP simulations, *J. Clim.*, *28*, 5549–5574.
Skamarock, W., J. Klemp, J. Dudhia, D. Gill, and D. Barker (2005), Coauthors, 2008: A description of the Advanced Research WRF Version 3. NCAR Technical Note, *Tech. Rep. NCAR/TN–475+ STR*, Nat. Cent. Atmos. Res., Boulder, Colo.
Skamarock, W. C., J. B. Klemp, M. G. Duda, L. D. Fowler, S.-H. Park, and T. D. Ringler (2012), A multiscale nonhydrostatic atmospheric model using centroidal Voronoi tesselations and C-grid staggering, *Mon. Weather Rev.*, *140*(9), 3090–3105.
Soares, P. M., R. M. Cardoso, P. M. Miranda, J. de Medeiros, M. Belo-Pereira, and F. Espirito-Santo (2012), WRF high resolution dynamical downscaling of ERA-Interim for Portugal, *Clim. Dyn.*, *39*(9–10), 2497–2522.
Solomon, S. (2007), *Climate Change 2007—The Physical Science Basis: Working Group I Contribution to the Fourth Assessment Report of the IPCC*, vol. *4*, Cambridge Univ. Press, Cambridge, U. K.
Staniforth, A. N., and H. L. Mitchell (1978), A variable-resolution finite-element technique for regional forecasting with the primitive equations, *Mon. Weather Rev.*, *106*(4), 439–447.
Stauffer, D. R., and N. L. Seaman (1990), Use of four-dimensional data assimilation in a limited-area mesoscale model. Part I: Experiments with synoptic-scale data, *Mon. Weather Rev.*, *118*(6), 1250–1277.
Sun, F., D. Walton, and A. Hall (2015), A hybrid dynamical-statistical downscaling technique, Part II: End-of-century warming projections predict a new climate state in the Los Angeles region, *J. Clim.*, *28*, 4618–4636.
Taylor, M. A. (2011), Conservation of mass and energy for the moist atmospheric primitive equations on unstructured grids, in *Numerical Techniques for Global Atmospheric Models*, pp. 357–380, Springer, Berlin, Germany.
Taylor, M. A., and A. Fournier (2010), A compatible and conservative spectral element method on unstructured grids, *J. Comput. Phys.*, *229*(17), 5879–5895.
Thornton, P. E., S. W. Running, and M. A. White (1997), Generating surfaces of daily meteorological variables over large regions of complex terrain, *J. Hydrol.*, *190*(3), 214–251.
Thornton, P. E., M. M. Thornton, B. W. Mayer, N. Wilhelmi, Y. Wei, R. Devarakonda, and R. B. Cook (2014), Daymet: Daily surface weather data on a 1-km grid for North America, Version 2, technical report, Oak Ridge Natl. Lab, Distributed Active Archive Center for Biogeochemical Dynamics (DAAC), Oak Ridge, Tennessee
Ullrich, P. A. (2014), *SQuadGen: Spherical Quadrilateral Grid Generator*, University of California, Davis, Climate and Global Change Group, Davis, Calif. [Available at http://climate.ucdavis.edu/squadgen.php.]
Warner, T. T., R. A. Peterson, and R. E. Treadon (1997), A tutorial on lateral boundary conditions as a basic and potentially serious limitation to regional numerical weather prediction, *Bull. Am. Meteorol. Soc.*, *78*(11), 2599–2617.
Wehner, M. F., R. L. Smith, G. Bala, and P. Duffy (2010), The effect of horizontal resolution on simulation of very extreme US precipitation events in a global atmosphere model, *Clim. Dyn.*, *34*(2–3), 241–247.
Wehner, M. F., et al. (2014), The effect of horizontal resolution on simulation quality in the Community Atmospheric Model, CAM5.1, *J. Model. Earth. Syst.*, *6*, 980–997, doi:10.1002/2013MS000276.
Wise, E. K. (2012), Hydroclimatology of the US Intermountain West, *Prog. Phys. Geogr.*, *36*(4), 458–479.
Zarzycki, C. M., and C. Jablonowski (2015), Experimental tropical cyclone forecasts using a variable-resolution global model, *Mon. Weather Rev.*, *143*(10), 4012–4037.
Zarzycki, C. M., M. N. Levy, C. Jablonowski, J. R. Overfelt, M. A. Taylor, and P. A. Ullrich (2014a), Aquaplanet experiments using CAM's variable-resolution dynamical core, *J. Clim.*, *27*(14), 5481–5503.
Zarzycki, C. M., C. Jablonowski, and M. A. Taylor (2014b), Using variable-resolution meshes to model tropical cyclones in the Community Atmosphere Model, *Mon. Weather Rev.*, *142*(3), 1221–1239.
Zarzycki, C. M., C. Jablonowski, D. R. Thatcher, and M. A. Taylor (2015), Effects of localized grid refinement on the general circulation and climatology in the Community Atmosphere Model, *J. Clim.*, *28*(7), 2777–2803.
Zhang, G. J., and N. A. McFarlane (1995), Sensitivity of climate simulations to the parameterization of cumulus convection in the Canadian Climate Centre general circulation model, *Atmos. Ocean*, *33*(3), 407–446.